Title

The remarkable crystal chemistry of the Ca14AlSb11 structure type, magnetic and thermoelectric properties

Authors

Hu, Yufei
Cerretti, Giacomo
Wille, Elizabeth L Kunz
et al.

Publication Date

2019-03-01

DOI

10.1016/j.jssc.2018.12.037

The Remarkable Crystal Chemistry of the $Ca_{14}AlSb_{11}$ Structure Type, Magnetic and Thermoelectric Properties

Yufei Hu,[1] Giacomo Cerretti,[2] Elizabeth L. Kunz Wille,[1] Sabah K. Bux,[2] and Susan M. Kauzlarich[1*]

[1]Chemistry Department, One Shields Ave, University of California, Davis, CA 95616

[2]Power and Sensors Systems Section, Jet Propulsion Laboratory, California Institute of Technology, 4800 Oak Grove Drive, Pasadena, CA 91109, USA

*smkauzlarich@ucdavis.edu

Abstract

$Yb_{14}MnSb_{11}$ is a member of a remarkable structural family of compounds that are classified according to the concept of *Zintl*. This structure type, of which the prototype is $Ca_{14}AlSb_{11}$, provides a flexible framework for tuning structure-property relationships and hence the physical and chemical properties of compounds. Compounds within this family show exceptional high temperature thermoelectric performance at temperatures above 300 K and unique magnetic and transport behavior at temperatures below 300 K. This review provides an overview of the structure variants, the magnetic properties, and the thermoelectric properties. Suggestions for directions of future research are provided.

1. Introduction to *Zintl* Phase Compounds

Named after Eduard Zintl, *Zintl* phases are salt-like intermetallic compounds in which electrons can be considered as completely transferred from cations to anions.[1, 2] In *Zintl* phases, electronic configurations of both cations and anions usually follow valence rules to have stable electronic configurations. Different from alloys, in which constituent elements have no clear oxidation states and electrons are shared by all the elements like metals, *Zintl* phase compounds are composed by elements of which oxidation states can be assigned and electrons are considered to be transferred from the electropositive element to the more electronegative one. The first *Zintl* phases systematically studied were binary compounds and the constituent elements were alkali or alkaline earth elements as cations, and group 13–15 elements as anions.[1, 2] The compositions of these compounds are simple ratios of their oxidation states, indicating the oxidation states of composite elements obey the octet rule and *Zintl-Klemm* concept is strictly followed.[1, 2] There are two different directions of research that have expanded the development of *Zintl* phase compounds.

One active research area is to systematically explore more complex compositions such as $Ca_{11}Sb_{10}$, K_4Pb_9, Na_8Si_{46}, $Ca_{14}AlSb_{11}$ and KBa_2InAs_3.[3-7] The other direction is to replace the alkaline earth metals with divalent rare earth elements (Sm, Eu and Yb) along with the introduction of transition metals into structures, typically replacing the less electronegative metalloid in the anionic framework.[8-10] Combinations of these two directions led to compounds such as $Yb_{14}MnSb_{11}$, Pr_4MnSb_9, $Eu_{10}Mn_6Sb_{13}$, $Yb_9Zn_{4+x}Bi_9$ and $Cs_{13}Nb_2In_6As_{10}$.[11-16] The complexity of compositions can be combined with a small flexibility in electron counting. For example, $Yb_{14}MnSb_{11}$ and $Yb_9Zn_{4+x}Bi_9$ do not strictly follow the *Zintl-Klemm* concept. $Yb_{14}MnSb_{11}$ has Mn^{2+} instead of a group 13 element such as in $Ca_{14}AlSb_{11}$ and therefore is electron deficient,[17] and $Yb_9Zn_{4+x}Sb_9$ has interstitial Zn atoms which can be compositionally varied to achieve specific properties.[18] At the same time, the total number of valence electrons within an identical *Zintl* phase structure type with different elements may also vary slightly but the variance can be quite small and limited for many structure types that can be described by the *Zintl* concept. Therefore, with the introduction of transition elements, new electronic properties are possible, but complete transfer of electrons and clear counting of valence electrons remains a criterion for describing transition and rare earth metal containing *Zintl* phase compounds.

Binary *Zintl* phase compounds which have compositions of simple ratios of elements usually adopt the structures of known oxides or halides, in which anions and cations are isolated in the structure with no covalent bonding.[2, 19] Both isolated anions, polyanions or clusters in *Zintl* phase compounds can provide complex compositions such as those represented by $Ca_{11}Sb_{10}$ and K_4Pb_9.[3, 4] Polyanions or clusters are formed to compensate for lack of enough electrons from the electropositive element to satisfy valence to form a simple one atom anion. Sb forms Sb-Sb single bonds in the $Ca_{11}Sb_{10}$ structure type resulting in Sb_2^{4-} and Sb_4^{2-} polyanions in the structure.[3] The *Zintl* electron counting provides the following charge balanced scenario: $11Ca^{2+} + 4Sb^{3-} + 2Sb_2^{4-} + Sb_4^{2-}$. Two types of clusters exist in K_4Pb_9 with the same formal oxidation state: a monocapped square antiprism and a tricapped trigonal prism of Pb_9^{4-}.[4] The *Zintl* electron counting works for double the formula, K_8Pb_9, providing $8K^+ + 2Pb_9^{4-}$. The polyanions or clusters can combine from infinite units or a framework structure. For example, anionic clathrates such as Na_8Si_{46} have an infinite framework of silicon with sodium filling the cages.[5] Ternary and quaternary *Zintl* phases can have even more complex structures. KBa_2InAs_3 has both $[In_2As_7]^{13-}$ isolated clusters and one dimensional infinite chains of $[In_2As_5]^{7-}$.[7] All the alkali and alkali earth metals are isolated as electron donors with no covalent bonding to the anions. The introduction of rare earth elements

and transition metals to *Zintl* phases pioneered by the Kauzlarich group lead to more possibilities.[8-10, 20] Rare earth elements that can have a 2+ oxidation state (Sm, Eu, Yb) can replace alkali or alkaline earth metals, and transition metals can replace the main group metalloid elements in *Zintl* structures. For example, $Yb_{11}Sb_{10}$ and $Yb_{14}MnSb_{11}$ are iso-structural to known *Zintl* phases, $Ca_{11}Sb_{10}$ and $Ca_{14}AlSb_{11}$.[11, 21] New structure types were also discovered due to the introduction of transition elements. For example, Pr_4MnSb_9, $Ca_{21}Mn_4Sb_{18}$, $Eu_{10}Mn_6Sb_{13}$, $Yb_9Zn_4Bi_9$, and $Cs_{13}Nb_2In_6As_{10}$ are all new structure types that have no exact main group metalloid analog.[13, 14, 22-24]

Zintl phases containing transition and *RE* metals have been shown to have unusual and unique magnetic properties,[8-10, 20] and many *Zintl* phases have found application as thermoelectric materials.[17, 25-27] The first phases defined as *Zintl* compounds consisted of main group elements and were typically diamagnetic or weakly paramagnetic.[19, 28, 29] However, the introduction of rare earth elements and transition elements are able to change the properties.[30, 31] As transition metals or rare earth ions may have unpaired electrons, *Zintl* compounds consisting of such elements can be magnetic such as ferro-, ferri- or antiferromagnetic. At the same time, these compounds can be semimetallic or metallic. One reason for that is the flexibility of electron count caused by the introduction of transition metals. Another reason is the contributions from *d*- and *f*-orbitals of the transition and rare earth metals. They are sometime underestimated by theoretical calculations due to the presumably small contribution of *d*-orbitals at the Fermi-level, compared with the *p*-orbitals and the difficulty in calculating *f*-orbitals. However, their presence may be important to the electronic bands near Fermi-level as *Zintl* phase compounds containing these high degeneracy orbitals have dramatically different properties from the analogs without *d*- and *f*-orbitals in the structures.

2. $A_{14}MPn_{11}$ Structure Type

As a structure type of *Zintl* phase compounds, the first analog of $A_{14}MPn_{11}$ was $Ca_{14}AlSb_{11}$ discovered in 1984 and since then more than 30 derivatives have been found.[6, 32] The structure of $A_{14}MPn_{11}$ (Figure 1) crystallizes in the space group $I4_1/acd$ and there are eight formula units, 208 atoms in total, in one unit cell. The structure can be described by the *Zintl* concept[6, 29] as follows: each formula unit is charge balanced as 14 A^{2+} + $[MPn_4]^{9-}$ + Pn_3^{7-} + 4 Pn^{3-}. Combinations of different elements lead to gradual changes in structure, e.g. unit cell parameters, bond angles, bond lengths of the $[MPn_4]^{9-}$ tetrahedral clusters and bond length of Pn_3^{7-}. All the published $A_{14}MPn_{11}$ compounds are listed in Table 1 with their structure information, and the volumes as a function of

ionic radii are plotted in Figure 2. It is immediately clear that while the ionic radii of Yb is slightly larger than Ca, in these structures the volume of the Yb containing compounds are consistently smaller for the same metal, M, and pnicogen, Pn. This may suggest more covalency in the Yb containing structure.[33] Table 1 is limited to structures of single elements on each site, so none of the solid solution structures are provided. To date, only the heavier alkaline earth elements, Ca, Sr and Ba, as well as the normal 2+ rare earth cations, Eu and Yb, have been reported as single elements on the A site.[30] Ca^{2+} (1.00 Å), Sr^{2+} (1.18 Å) and Ba^{2+} (1.36 Å) are large alkali earth ions and Yb^{2+} (1.02 Å) and Eu^{2+} (1.17 Å) are respectively similar in size to Ca^{2+} and Sr^{2+}.[34] The unit cell parameters are strongly related to the elements, or the size of ions. From Ca to Ba, *a*, *c* and *V* linearly increase when Pn is fixed, while the *c*/*a* values (Table 1) decrease from Ca to Ba. The only exception is $Ca_{14}CdSb_{11}$ which has an exceptionally large *c* value and *c*/*a* value. According to the trend in the system, the reported unit cell parameters of $Ca_{14}CdSb_{11}$ may require an additional structure solution.[35] There may be interstitial Cd or Sb atoms in the structure, altering the unit cell parameters as has been indicated for $Sr_{14}CdSb_{11}$.[36] For the two rare earth elements, Eu and Yb, unit cell parameters also show similar dependence on the sizes of their ions.[34] Eu^{2+} (1.17 Å) is similar in size to Sr^{2+} (1.18 Å), and therefore the unit cell parameters of Eu analogs are most similar to but slightly smaller than those of Sr.

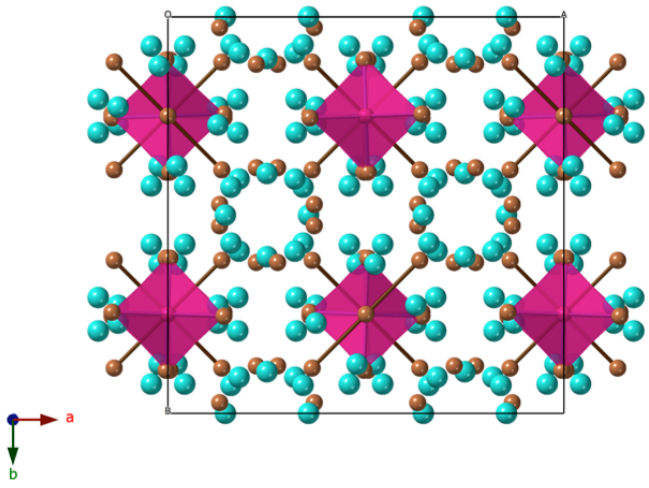

Figure 1. Unit cell of $A_{14}MPn_{11}$ projected along the *c*-axis. A and Pn atoms are represented by blue and brown spheres, Pn_3^{7-} ions are shown with brown bonds and the pink tetrahedra are $[MPn_4]^{9-}$ clusters.

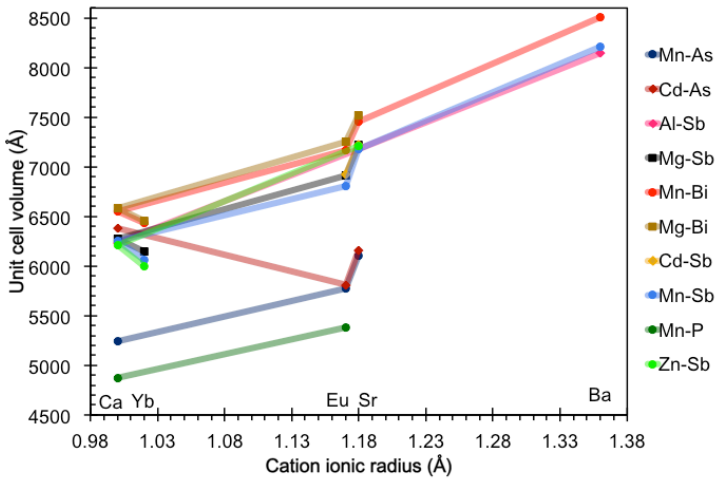

Figure 2. Volume vs cation ionic radius for $A_{14}MPn_{11}$.

Table 1. List of published $A_{14}MPn_{11}$ compounds with single crystal structure results. Data are for room temperature, unless otherwise noted.

Compound	*a* (Å)	*c* (Å)	*V* (Å)	*c*/*a*	M-Pn bond length (Å)	Pn-M-Pn bond angles	Pn-M-Pn bond angle ratio	Pn-Pn bond length (Å)[#]	Ref
P									
*$Ca_{14}GaP_{11}$	15.347	20.762	4890	1.353	2.541	107.93/112.59	1.043	2.930	[37]
*$Ca_{14}MnP_{11}$¶	15.326	20.757	4875	1.354	2.543	108.05/112.36	1.040	2.929	[38]
*$Eu_{14}MnP_{11}$‡	15.930	21.213	5383	1.332	2.585	106.60/115.39	1.082	3.059	[39]
As									
*$Ca_{14}GaAs_{11}$‡	15.642	21.175	5181	1.354	2.546	107.80/113.00	1.048	2.956	[40]
*$Ca_{14}MnAs_{11}$‡	15.785	21.041	5243	1.333	2.603	107.10/114.40	1.068	3.019	[41]
*$Eu_{14}MnAs_{11}$‡	16.318	21.684	5774	1.329	2.646	106.24/116.14	1.093	3.134	[39]
*$Eu_{13}\square NbAs_{11}$	16.329	21.973	5859	1.346	2.511	107.06/114.40	1.069	3.053	[42]
*$Sr_{13}\square NbAs_{11}$	16.498	22.131	6024	1.341	2.508	107.14/114.23	1.066	3.093	[42]
*$Sr_{14}CdAs_{11}^{fl+}$	16.615	22.321	6162	1.343	2.758	107.10/114.38	1.068	3.191	[36]
*$Eu_{14}CdAs_{11}^{fl+}$	16.306	21.860	5812	1.341	2.745	107.08/114.38	1.073	3.162	[36]
*$Sr_{14}GaAs_{11}$‡	16.513	22.140	6037	1.341	2.613	106.90/114.70	1.073	3.108	[43]
*$Sr_{14}MnAs_{11}$‡	16.575	22.229	6107	1.341	2.683	106.90/114.70	1.073	3.100	[41]
Sb									
$Yb_{14}ZnSb_{11}$¶	16.562	21.859	5996	1.320	2.726	105.60/117.60	1.114	3.175	[44]
$Yb_{14}MnSb_{11}$@	16.615	21.948	6059	1.321	2.750	105.60/117.50	1.113	3.195	[11]
$Yb_{14}MgSb_{11}$¶	16.625	22.240	6145	1.338	2.806	106.80/114.97	1.077	3.196	[45]
$Ca_{14}AlSb_{11}$	16.676	22.423	6236	1.345	2.718	107.30/114.00	1.062	3.196	[6]
$Ca_{14}MnSb_{11}$‡	16.742	22.314	6254	1.333	2.759	106.60/115.30	1.082	3.215	[41]
$Ca_{14}ZnSb_{11}$‡	16.790	22.022	6208	1.312	2.752	105.26/118.96	1.130	3.231	[35]
$Ca_{14}CdSb_{11}$‡	16.583	23.167	6371	1.397	2.882	107.63/110.40	1.026	3.180	[35]
$Ca_{14}MgSb_{11}$¶	16.681	22.561	6278	1.353	2.809	107.94/112.58	1.023	3.220	[45]

$Eu_{14}MnSb_{11}$@	17.300	22.746	6808	1.315	2.790	105.10/118.60	1.128	3.258	46
$Eu_{14}MgSb_{11}$	17.344	22.981	6913	1.325	2.875	106.73/115.10	1.078	3.342	47
$Sr_{14}Al_{0.85}Sb_{11}$‡	17.542	23.330	7179	1.330	2.833	107.00/114.60	1.071	3.302	48
$Sr_{14}MnSb_{11}$‡	17.530	23.354	7177	1.332	2.838	106.40/115.90	1.089	3.310	41
$Sr_{14}MgSb_{11}$+	17.569	23.399	7223	1.332	2.875	106.73/115.10	1.078	3.342	47
*$Sr_{14}ZnSb_{11}$‡	17.632	23.174	7205	1.314	2.806	104.96/118.96	1.133	3.338	35
$Eu_{14}InSb_{11}$@	17.289	22.770	6808	1.317	2.865	107.10/114.40	1.068	3.257	46
*$Sr_{14}CdSb_{11}$‡	17.611	23.277	7219	1.322	2.909	105.00/118.85	1.132	3.359	35
*$Sr_{14}Cd_{1.3}Sb_{11}$fl	17.616	23.203	7200	1.317	2.898	105.00/118/00	1.132	3.34	36
$Eu_{14}CdSb_{11}$fl	17.403	22.862	6924	1.314	2.885	104.62/120.56	1.152	3.264	36
$Ba_{14}Al_{0.96}Sb_{11}$‡	18.360	24.150	8141	1.315	2.799	105.40/117.90	1.119	3.370	48
*$Ba_{14}MnSb_{11}$‡	18.395	24.266	8211	1.319	2.872	105.10/118.70	1.129	3.418	41
Bi									
$Yb_{14}MgBi_{11}$¶	16.974	22.399	6454	1.320	2.849	105.62/117.48	1.112	3.345	49
$Yb_{14}MnBi_{11}$@	17.000	22.259	6433	1.309	2.803	104.70/119.40	1.140	3.336	11
$Ca_{14}MnBi_{11}$‡	17.066	22.498	6553	1.318	2.814	105.40/118.00	1.120	3.297	50
$Ca_{14}MgBi_{11}$	17.047	22.665	6587	1.330	2.861	106.36/115.88	1.090	3.358	51
$Eu_{14}InBi_{11}$^	17.672	23.110	7219	1.308	--	--	--	--	46
$Eu_{14}MnBi_{11}$@	17.633	23.055	7168	1.307	2.862	104.69/119.54	1.142	3.397	46
$Eu_{14}MgBi_{11}$	17.666	23.244	7254	1.316	2.858	105.46/117.83	1.117	3.362	51
$Sr_{14}MnBi_{11}$‡	17.847	23.442	7460	1.314	2.889	105.00/118.70	1.130	3.425	50
$Sr_{14}MgBi_{11}$	17.854	23.580	7517	1.321	2.928	105.70/117.31	1.110	3.445	51
$Ba_{14}MnBi_{11}$‡	18.665	24.429	8511	1.309	2.935	104.50/119.90	1.147	3.498	50

#Average distance from the center for a split site Pn(4).
*Pn(4) atom, the central Pn atom of Pn_3^{7-} unit has split sites.
+Pn(3) atom exhibits positional disorder, modelled as a majority and a minority site
‡ T, K = 130
¶T, K = 90
flT, K = 200
@ T, K = 143
^ Lattice parameters from powder diffraction data.

The atom numbering for $A_{14}MPn_{11}$ is provided in Figure 3. This view also shows how the tetrahedra and the three-atom unit alternate down the *c* axis. The Pn in the tetrahedra is designated as Pn2, and the three-atom linear anion is defined as Pn1-Pn4-Pn1. The Pn^{3-} (Pn3) anions are considered isolated as there are no reasonable distances that might be considered Pn-Pn bonding, and the anions are six-coordinated by the A^{2+} cations. The distance between M atoms in the $[MPn_4]^{9-}$ cluster is around 10 Å and the $[MPn_4]^{9-}$ cluster is compressed along the *c*-direction and distorted from an ideal tetrahedral angle of 109˚. Bond distances and the Pn3 site will be discussed in more detail below.

The bonding of Pn_3^{7-} is considered to be a three-center-four-electron bond, similar to that of I_3^-.[45, 52-54] The tetrahedron and Pn_3^{7-} alternate down the *c* axis as shown in Figure 3. This structural feature relates to the size of ions is the disorder and order of the central Pn atom (Pn4) in Pn_3^{7-} units. The both Pn4 and Pn1 of the Pn_3^{7-} linear unit may have split sites in some analogs such as phosphides[37, 39, 55-57] and arsenides.[36, 40, 41, 43] This can manifest in large thermal ellipsoids in single crystal X-ray diffraction data refinement and typically various disorder models are employed to account for the electron density. In the P and As containing analogs, the central Pn atom in the Pn_3^{7-} is best modeled as a split site. The central Pn4 atom of the Pn_3^{7-} unit deviates from the ideal fully-occupied *8b* sites and is split into the *16f* sites with 50% occupancy. The Pn-Pn bond lengths of Pn_3^{7-} are also affected by the A size and unit cell parameters. When Pn-Pn bonds are surrounded by large A ions and Pn atoms are too small to form stable three-center-four-electron bonding,[58] the Pn4 atom deviates from the original central site to form one strong Pn-Pn bond and one weak Pn-Pn bond, lowering the total energy and stabilizing the structure. In the case of $Ba_{14}GaP_{11}$, both the P4 and P1 sites are best described by split sites. In the As analogs, the central As4 site is described as split; in the Sb analogs, only the large cations, such as Sr and Ba, lead to the splitting of the Sb4 site. To date, none of the reported Bi compounds show a split site. Figure 4 shows a summary of the possibilities for structural models of the Pn_3^{7-} unit.[55] Typically, the most common one employed uses a split site on the central Pn atom (Pn4).

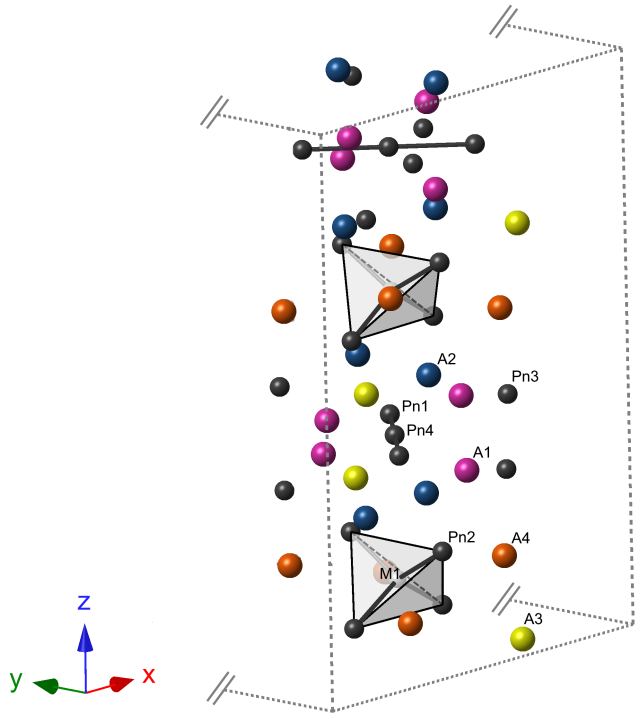

Figure 3. A view of a portion of the $A_{14}MPn_{11}$ structure showing the MPn_4 tetrahedra (Pn = Pn2), the three-atom trimer (Pn1-Pn4-Pn1), the isolated Pn3 has no bonds to it and all the Pn atoms are indicated in brown. A1 indicated in teal, A2, A3, and A4 in green, blue and yellow, respectively.

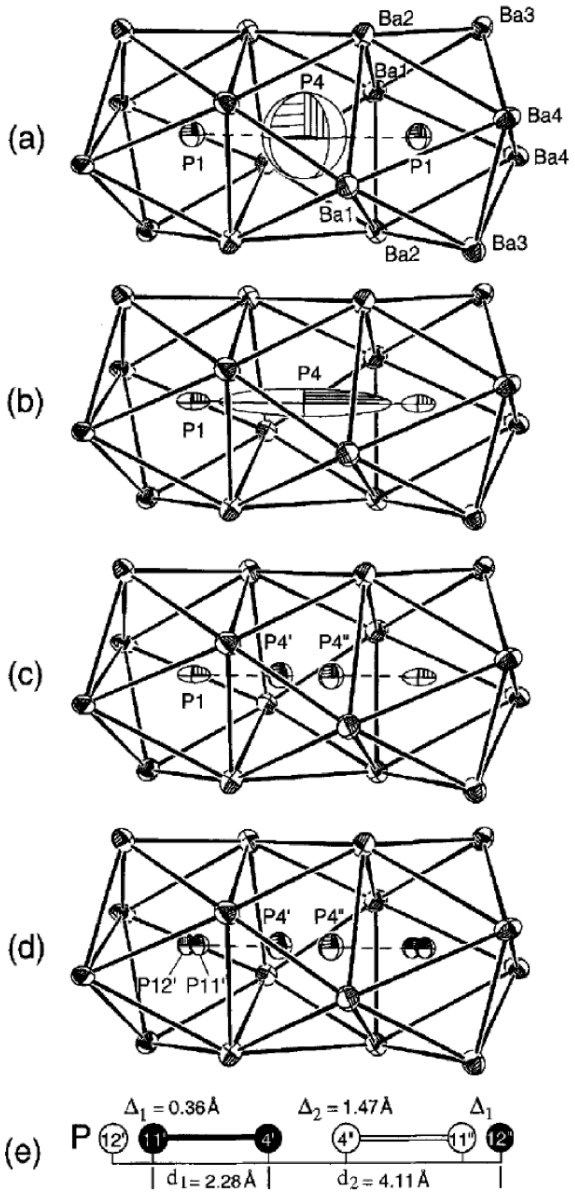

Figure 4. Various models for the P_3^{7-} anion employed in the structure solution for $Ba_{14}InP_{11}$. The Ba^{2+} cations surrounding the P_3^{7-} anion in a central tetragonal antiprism sharing quadrangular faces with two bicapped trigonal prisms (16 Ba cations total) are shown. Various models that were used to refine the single crystal data are shown in (a)–(e). The final model employed for $Ba_{14}InP_{11}$ was (d) and distances are provided in (e). Either (c) or (d) models of split sites have been employed in other Pn = P, As containing $A_{14}MPn_{11}$ compounds. Image reproduced with permission from Carrillo-Cabrera, W.; Somer, M.; Peters, K.; Schnering, H. G. v., Synthesis, Structure and Vibrational Spectra of Ba141nP11. *Chem. Ber.* **1996,** *129*, 1015-1023, ref [55].

There are four A sites and each one is surrounded by six Pn atoms in pseudo octahedral coordination as shown in Figure 5. These pseudo octahedra are significantly distorted with the

exception of A3 site. From a merely cationic perspective, the crystal structure can be conceptualized as a combination of four different types of distorted APn_6 octahedra that generate polyhedral chains along the *c*-direction (Figure 5). Site preferences are observed in the occupancy of the cation sites when doping or alloying on the A position.[31, 59-66] The tendency is for smaller atoms to prefer the A1 and A3 sites, and for larger atoms to prefer the A2 and A4 sites. This can be understood through the Hirshfeld surface analysis of chemical bonding. A2 and A4 show the largest atomic Hirshfeld surface volumes, while A1 and A3 have the smallest.[33]

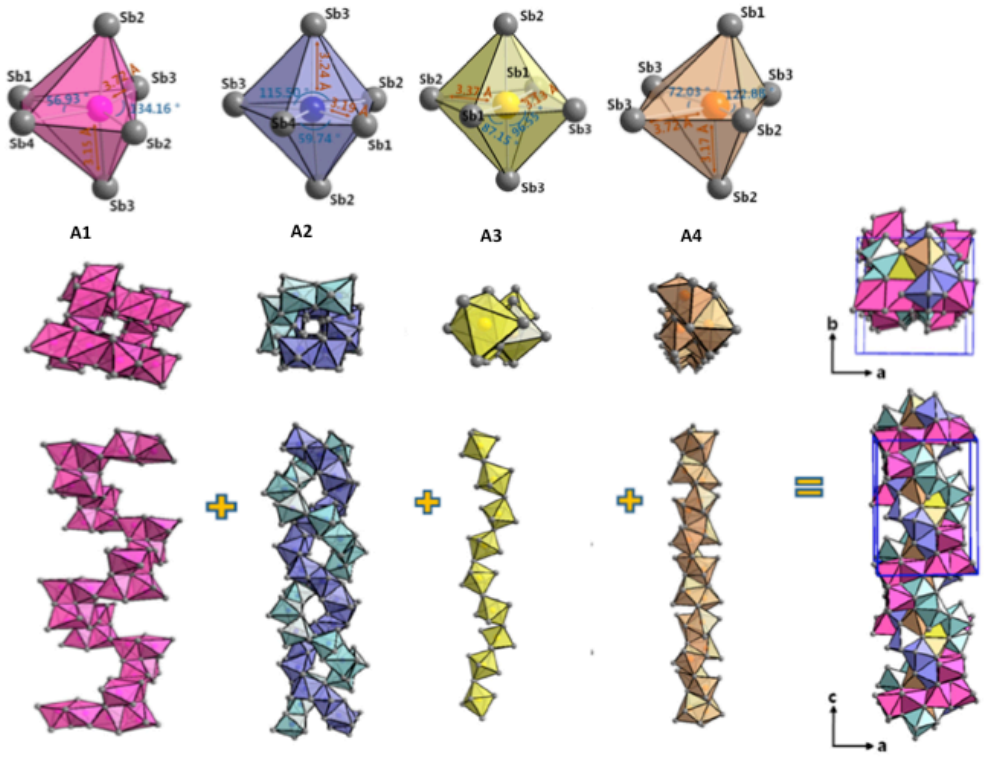

Figure 5. Representation of the four type of distorted APn_6 octahedra formed by the four different color-coded cationic sites (A1 (pink), A2 (blue), A3 (yellow), A4 (orange)) with the relative bonding lengths and angles. Each type of octahedron forms a chain that propagates through the crystal structure along the *c*-direction, shown below. Therefore, each cationic site is responsible for a different octahedral pattern (multicolored image on far right). Images adapted and reproduced with permission from Nam, G.; Jang, E.; Jo, H.; Han, M. K.; Kim, S. J.; Ok, K. M.; You, T. S., Cationic Site-Preference in the $Yb_{14-x}Ca_xAlSb_{11}$ ($4.81 \leq x \leq 10.57$) Series: Theoretical and Experimental Studies. Materials (Basel) **2016,** 9, 553. Copyright 2016 by the authors, ref [67].

The M site has been substituted by the main group 13 elements, Al, Ga and In, and the transition metals Mn, Zn, Nb and Cd, and the alkaline earth metal Mg.[30] Figures 6-8 show the c/a

ratio and the M-Pn bond distances for $A_{14}MPn_{11}$, M = Mn, Mg, Zn, Cd, Al, Ga. The metal atom M =Al, Ga and In, can be considered to be formally 3+ in the $[MPn_4]^{9-}$ tetrahedron and Mg, Mn, Zn and Cd are considered to be 2+. The Mn in $Yb_{14}MnSb_{11}$ has been shown to be Mn^{2+} by X-ray Magnetic Circular Dichroism (XMCD) and XPS spectroscopies.[44, 68] These results are further supported by neutron diffraction and spectroscopy.[69] Mg is a special element for the M site,[45] because as an alkaline earth element it was assumed that it might prefer the A site. However, any attempt to synthesize compounds with A = Mg never succeeded. Instead, Mg was discovered to occupy the M site in the structure.[45] This can be attributed to the small size of Mg^{2+}, its preference for a tetrahedral coordination geometry, and its chemical similarity to Al. The radius of Mg^{2+} (0.57 Å) is similar to those of Mn^{2+} (0.66 Å) and Zn^{2+} (0.60 Å) and is much smaller than the other alkaline earth ions that occupy the A sites.[34] Figures 6-8 show that the *c*/*a* values of Eu and Yb are respectively smaller than those of Sr and Ca. The difference in unit cell parameters and *c*/*a* values may be caused by ionic polarization of the alkaline earth as compared to the rare earth ion. From P to Bi, similar trends are also observed, that is *c*/*a* values decrease with larger ionic radii. As can be seen from Figures 6-8, bond lengths of M-Pn in MPn_4 tetrahedron and Pn-Pn in the Pn_3^{7-} unit increase with increasing Pn size. $Ca_{14}MgSb_{11}$ and $Yb_{14}MgSb_{11}$ are the first examples of the Mg containing compounds in this structure type.[45] They have larger unit cells compared to other $(Ca/Yb)_{14}MSb_{11}$ compounds, although Mg has a smaller ionic radius compared to the other metals occupying the M position (Cd, Mn, Zn). This can be explained by a reduced distortion of the $MgSb_4$ tetrahedra. Two recent examples of Mg containing compounds are $Sr_{14}MgSb_{11}$ and $Eu_{14}MgSb_{11}$.[47] Although Sr and Eu are similar in charge and size, the two compounds present some crystallographic differences. They both crystalize in the tetragonal crystal group $I4_1/acd$, but the Sr analog shows disorder of the Sb3 atom, which results in a long Sb-Sb interaction, similar what has been described for $Sr_{14}ZnSb_{11}$.[35] From the *Zintl* perspective, the $Sr_{14}MSb_{11}$ M = Mg, Zn is one electron deficient compared to $Ca_{14}AlSb_{11}$, due to the difference between the oxidation states of Mg^{2+}, Zn^{2+} and Al^{3+}. This deficiency could be the main reason for the long Sb-Sb distance between Sb3 atoms in the $Sr_{14}MgSb_{11}$ compound, where one can envision a bond order of one half that would compensate for the loss of one electron.[35, 47] With this scenario, one might expect $Eu_{14}MgSb_{11}$ to show the same structural distortion, but it is not apparent.[47] However, the $MgSb_4$ tetrahedra in $Eu_{14}MgSb_{11}$ are characterized by a larger deviation from the ideal tetrahedral angle (109.5°). These structural differences deeply affect the electronic conduction with $Eu_{14}MgSb_{11}$ being more conductive than $Sr_{14}MgSb_{11}$.[47] Other variants of Mg containing compounds have been

recently discovered. $A_{14}MgBi_{11}$ (A = Yb, Ca, Eu, Sr)[49, 51] are isostructural to $Ca_{14}AlSb_{11}$ and therefore crystalize in the same space group (*I4₁/acd*). While the Sb analogs present several crystal distortions, the bismuth compounds appear to be overall more ordered. There is a strict correlation between the Mg-Bi bond lengths within the $MgBi_4$ tetrahedra and the size of the A cation. Indeed, similarly to what observed for the Mn containing bismuthates, the Mg-Bi bonding increases with increasing ionic radius of the A cation. Another trend that can be observed is the distortion of the $MgBi_4$ tetrahedra, which increases when the A site is occupied by rare earth elements rather than alkali earth metals, and this is true for all the Mg containing compounds, independently from the Pn atom. In a more general sense, Pn are the heavier pnicogen elements such as P, As, Sb and Bi, which are formally trivalent anions in the structure. Among these four elements of the group 15, the Sb analogs are the most studied. The phosphorus containing analogs are the least studied to date.[37-39, 55, 56] The arsenic analogs are also relatively few in number and are certainly worth investigation.[39, 40, 42, 43, 52, 53, 57, 70] Although many analogs have been discovered with this structure type, still more possibilities remain unstudied. The first reason is that not all combinations of the elements mentioned above have been fully characterized; the second is that more compounds will be possible if a new element is introduced into this system.

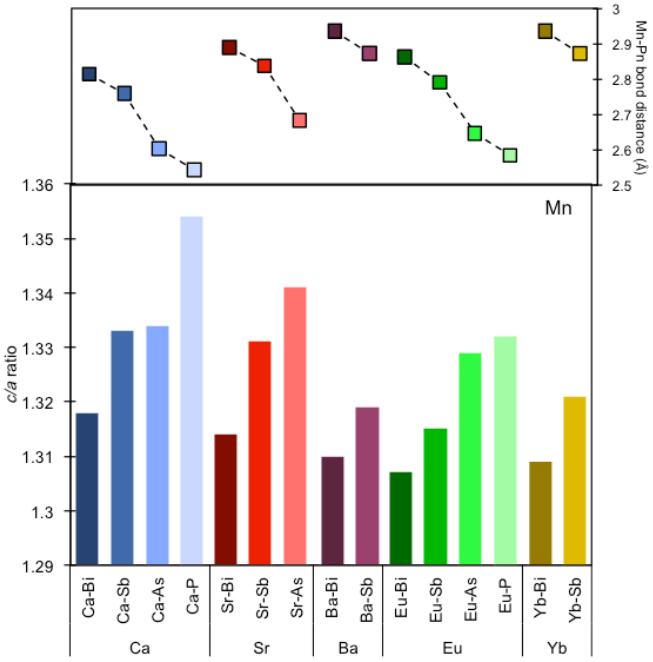

Figure 6. The c/a ratio and corresponding M-Pn bond lengths for $A_{14}MnPn_{11}$.

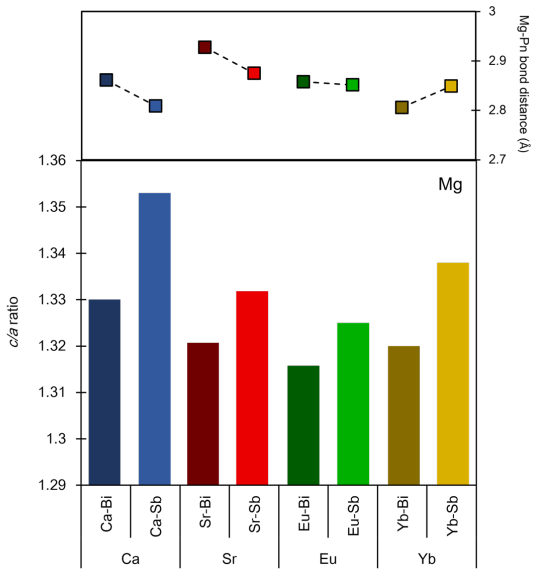

Figure 7. The c/a ratio and corresponding M-Pn bond lengths for $A_{14}MgPn_{11}$.

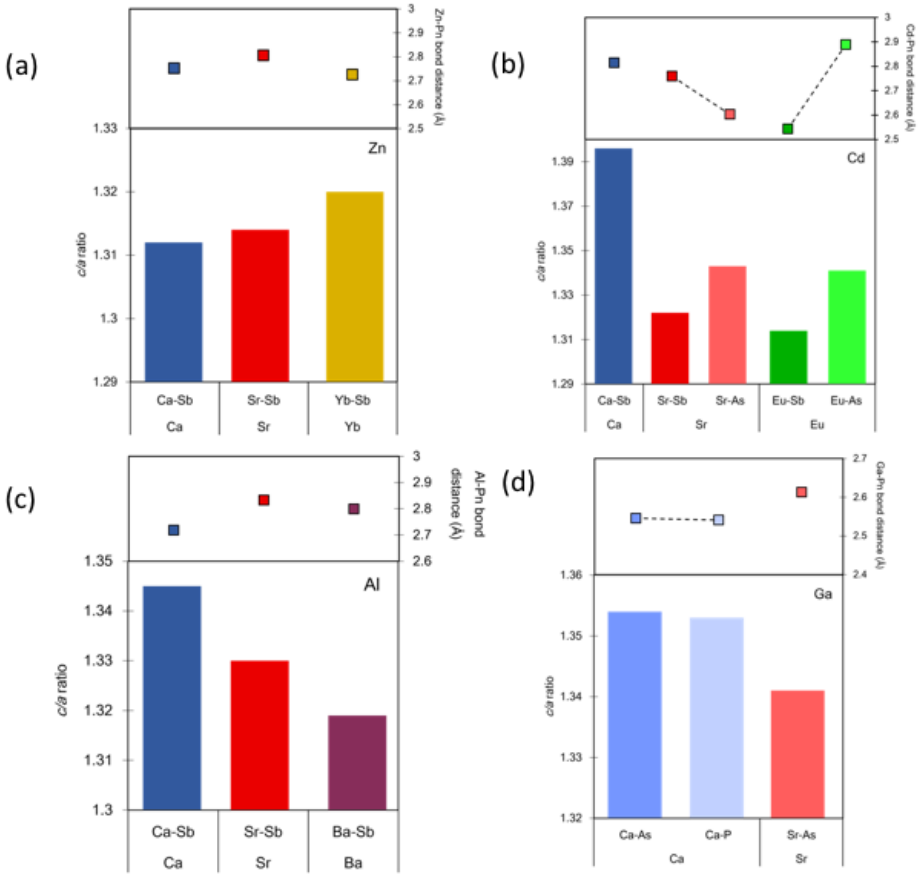

Figure 8. c/a and corresponding M-Pn bond lengths for $A_{14}MPn_{11}$, M = (a) Zn, (b) Cd (c) Al, and (d) Ga.

Two compounds containing Nb have been reported: $A_{13}\square NbAs_{11}$ (A = Eu and Sr, $\square$ = vacancy).[42] Here, the substitution of the M^{3+} atoms by Nb^{5+} results in the formation of vacancies to balance the charge count according to the *Zintl* concept. These vacancies occur in the A3 position, hence that site is only half filled. The A3 atoms are in coordination with the As1, As2, and As3, and form with As2 an almost linear Nb-As2-A3 chain. Therefore, the Sr3 (Eu3) atoms are the most strongly affected by the formal charge of the central atom M. So far, only structural information for these two compounds ($Sr_{13}\square NbAs_{11}$, $Eu_{13}\square NbAs_{11}$) has been reported.[42] The structure of $Ca_{14}Nb_xIn_{1-x}As_{11}$, ($x \approx 0.85$) has also been reported, but no properties.[71] In order to expand the number of Nb containing compounds of the $A_{14}MPn_{11}$ structure type, further studies are required. Synthesizing Eu/$Sr_{13}\square NbAs_{11}$ may be difficult as the crystals were discovered serendipitously by the reaction of the elements with the niobium container at elevated temperatures. In the publication of the structure of $Ca_{14}Nb_xIn_{1-x}As_{11}$, ($x \approx 0.85$), the authors reported that they were not able to optimize the synthesis to obtain a high yield for property measurements.[71] The fact that compounds with Nb have been prepared suggests more exotic compositions and as yet undiscovered compounds with other transition metals might be possible with this structure type. In addition to other transition metals, Group 14 elements may also be potential substituents in $A_{14}MPn_{11}$ structures. Sn^{2+} (1.18 Å) and Pb^{2+} (1.19 Å) are similar in size to Sr^{2+}(1.18 Å); Ge^{4+} (0.39 Å) and Sn^{4+} (0.55 Å) are respectively similar to Al^{3+} (0.39 Å) and Mn^{2+} (0.60 Å) in size.[34] The specialty of $A_{14}MPn_{11}$ structure type is its large flexibility and certainly more compositions will be forthcoming with continuing research.

Pn-M-Pn bond angles are also strongly related to Pn size (angles for Pn = Sb are shown in Figure 9; angles for Pn = Bi are shown in Figure 10). There is a rough trend between M elements and *c*/*a*, M-Pn bond lengths as well as Pn-M-Pn bond angles. Generally main group M elements and Mg lead to less distorted $[MPn_4]^{9-}$ tetrahedron (angles closer to 109˚) and therefore larger *c*/*a* values while transition metals such as Mn, Zn and Cd tend to have a more distorted tetrahedron. The M-Pn and Pn-Pn bond lengths increase with the size of A atoms, suggesting that the A cation has an impact on the bonding interactions. Pn-M-Pn bond angles show similar trends with both A and Pn atoms. This suggests that A atoms not only act as electron donors in the system, but they also have an effect on the MPn_4 tetrahedra and Pn_3^{7-} units, leading to a change in properties. The A-Pn interactions may be more important than previously assumed, although it is difficult to isolate the interactions. The studies of Eu and Sr as well as Yb and Ca phases provide some insight. Although Eu is similar to Sr in size, Eu analogs have smaller unit cell parameters than the Sr

analogs. Thus, Eu can be considered smaller than Sr in the $A_{14}MPn_{11}$ analogs. This is consistent with previous statement that the A ionic size lengthens the Pn-Pn bonds in Pn_3^{7-}. Among all the parameters previously discussed, *V* and Pn-Pn bond lengths strictly follow the trend that large ionic size provides larger values, while *c*/*a*, M-Pn bond lengths and Pn-M-Pn bond angles may have exceptions due to the effect of M atoms.

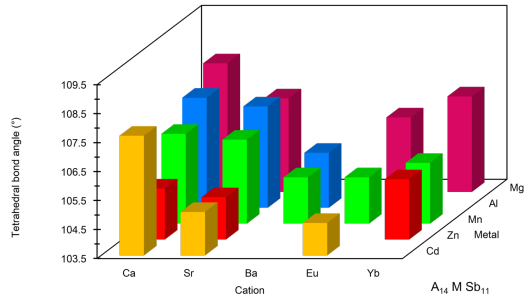

Figure 9. Sb-M-Sb bond angles for the $[MSb_4]^{9-}$ tetrahedra in $A_{14}MSb_{11}$.

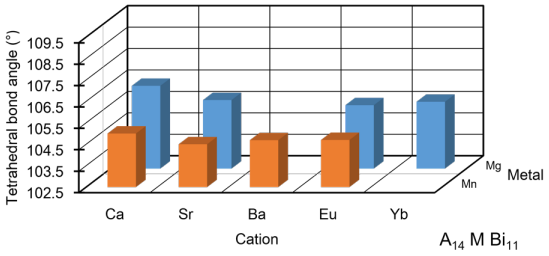

Figure 10. Bi-M-Bi bond angles for the $[MBi_4]^{9-}$ tetrahedra in $A_{14}MBi_{11}$.

Solid solutions of the A site were initially studied to investigate the magnetic properties of $Eu_{14-x}A_xMnSb_{11}$ where A = Ca, Sr, Ba.[72-74] The solid solution, $Yb_{14-x}Ca_xMnSb_{11}$ has also been studied in order to investigate the thermoelectric properties.[75-77] More recently, the solid solutions of the A site have focused on *RE* (rare earth) substitutions.[31, 59-66, 78] As mentioned above, the rare earth elements in the 3+ oxidation state (*RE*) show site preferences that depend upon size. The identity of the 3+ rare earth element affects the sublimation temperature and melting point with the lighter rare earths providing higher melting points and lower vapor pressures.[79] Additionally, the lighter rare earths affect the rate of oxidation, forming a protective oxide surface.[80] In the case of $A_{14-x}RE_xMSb_{11}$, the effect of a 3+ rare earth depends upon the *RE* cation and the element in the

A site The amount of *RE* appears to be limited to x ~ 0.5 in the case of $Yb_{14-x}RE_xMnSb_{11}$,[31, 59-64, 78] however, in the case of $Ca_{14-x}RE_xMnSb_{11}$ and $Ca_{14-x}RE_xMnBi_{11}$, the amount of x appears to be closer to 1.[65, 66] Solid solutions on the M site have focused on Mn-Zn and Mn-Al.[81-83] The only reported solid solution study of the Pn site is that of $Yb_{14}MnSb_{11-x}Bi_x$.[84] Dopants on the Pn site include Ge,[85] Te,[86] and Sn.[87]

3. Properties of $A_{14}MPn_{11}$ Compounds

3.1 Magnetic and Electrical Properties

$A_{14}MPn_{11}$ analogs compounds behave like either a typical or a heavily-doped *p*-type semiconductor, depending on the constituting elements. Generally speaking, the heavier Pn atoms provide higher conductivity since they will increase mobility in *p*-type semiconductors and decrease the band gap. In $A_{14}MPn_{11}$, the *p*-orbitals of the Pn atoms contribute most to the bands right below the Fermi-level (Figure 11). The antibonding orbitals of Pn_3^{7-} units dominate in the steep DOS peak in conduction band which is 0.5-1 eV above the valence band. The electronic structure of the series $A_{14}MnBi_{11}$ (A = Ca, Sr, Ba) was studied with a local-orbital based method within the local spin-density approximation in order to better understand the magnetic and transport properties.[54] The calculations show a gap between a bonding valence-band and an antibonding conduction-band continuum where the bonding bands lack one electron per formula unit of being filled, thus making them low carrier density p-type metals, as observed experimentally. The hole resides in the $MnBi_4$ tetrahedral cluster, and partially compensates for the high-spin d^5 Mn moment, leaving a net spin near $4\mu_B$ that is consistent with experiment. This appears to be the case for all of the Mn containing analogs, with the exception of the $Ca_{14}MnP_{11}$ analog where the Mn moment is closer to that expected for Mn^{2+}.[38] A view of the molecular units, the $MnBi_4$ cluster, and the Bi_3 unit is shown in Figure 12. These $MnBi_4$ clusters are composed of two independent interpenetrating networks of $MnBi_4$ clusters with ferromagnetic interactions within the same network and weaker couplings between the networks whose sign and magnitude are sensitive to materials parameters. Consistent with experiment, $Ca_{14}MnBi_{11}$ is calculated to be ferromagnetic, while for $Ba_{14}MnBi_{11}$ where experiments shown antiferromagnetism, the ferromagnetic and antiferromagnetic states are calculated to be degenerate. The band structure of the ferromagnetic states is very close to half metallic, suggesting that this structure type might show more exotic properties if appropriately doped or with a promising elemental composition. The majority of conduction bands are from the orbitals of the A atoms. Since the less

electronegative Pn atoms are larger and the bonding interactions are weaker, the energy difference between nonbonding and antibonding orbitals is small. Therefore, a smaller band gap and higher conductivity are achieved with less electronegative Pn atoms. On the aspect of A atoms, more electropositive A atoms increase the energy of conduction band and increase the band gap. Orbitals of more electropositive A atoms also hybridize with the antibonding orbitals of Pn_3^{7-} and increase the band gap.[54] For example, in $A_{14}MnPn_{11}$ (A = Ca, Sr, and Ba, Pn = As, Sb, and Bi), properties vary depending on the identity of both alkaline earth elements and pnicogen elements.[41, 50] $A_{14}MnAs_{11}$ show typical semiconductor behavior with the activation energy increasing from 0.18 eV for $Ca_{14}MnAs_{11}$ to 0.38 eV for $Ba_{14}MnAs_{11}$. In $A_{14}MPn_{11}$ compounds, P and As analogs are all semiconductors with $Eu_{14}CdAs_{11}$ as an exception. All Bi analogs are metallic while Sb analogs are either semiconducting or metallic. $A_{14}MSb_{11}$ (A = alkali earth metals, M = Mg and Al) are semiconductors as well as a few M = Mn, Zn and Cd analogs with very small band gaps. Carrier concentrations of Sb analogs vary from $10^{19}cm^{-3}$ to 10^{21} cm^{-3}.[45] $A_{14}MPn_{11}$ analogs tend to be more conductive when M is divalent transition metals. The reason is that divalent metals leave a hole in the structure and increase carrier concentration.[54] Group 13 elements can donate one more electron than other M elements, therefore their analogs tend to have smaller carrier concentration and to be semiconducting. Eu and Yb analogs tend to have smaller resistivity because they have higher electronegativity and their *f*-orbital may diffuse near the Fermi-level.

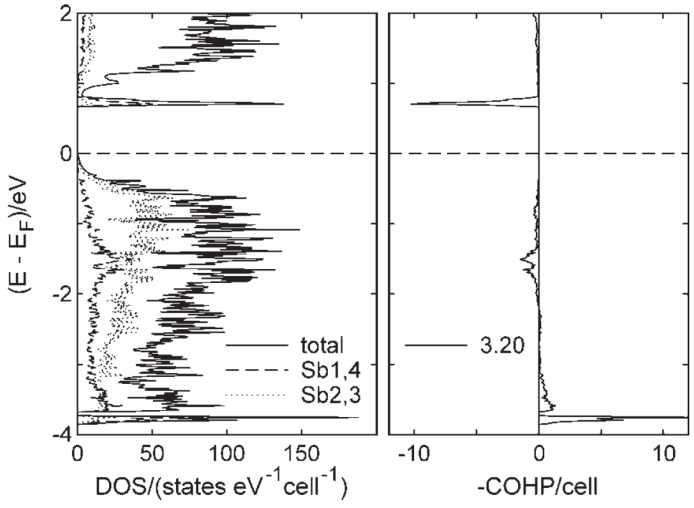

Figure 11. $Ca_{14}AlSb_{11}$ density of states (left) showing the Sb contributions and Sb-Sb crystal orbital Hamilton populations, COHP (right). Sb1 and Sb4 make up the three-atom linear unit. Sb2

is part of the tetrahedron and Sb3 is an isolated (6 coordinated by cations) atom. The COHP curve shows that the sharp peak above the Fermi level is an antibonding state from the three-atom linear unit. Image reproduced with permission from ref 88.

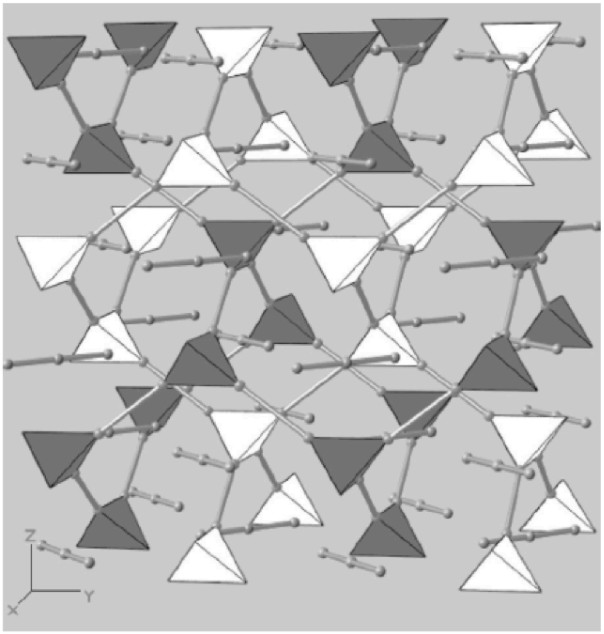

Figure 12. A view of the two interpenetrating sublattices of $MnBi_4$ tetrahedra with Bi_3 units of $Ca_{14}MnBi_{11}$, one shown as white and the other one grey. Reprinted Figure 1 with permission from [Sánchez-Portal, D.; Martin, R. M.; Kauzlarich, S. M.; Pickett, W. E., Bonding, moment formation, and magnetic interactions in$Ca_{14}MnBi_{11}$and $Ba_{14}MnBi_{11}$. *Physical Review B* **2002,** *65,* 144414.] Copyright 2002 by the American Physical Society. [54]

Magnetic properties of $A_{14}MPn_{11}$ analogs originates from the composite elements, namely Eu in A site and Mn in M site. The coupling of magnetic moments are strongly correlated with the electrical properties.[10] In $A_{14}MnPn_{11}$, the interactions between magnetic moments on Mn are believed to be conducted by carriers via Ruderman-Kittel-Kasuya-Yosida (RKKY) interactions due to the large distance between Mn atoms (~10 Å).[11, 41, 54] Higher carrier concentrations cause stronger interactions and higher transition temperatures. For example, $A_{14}MnSb_{11}$ analogs are ferromagnetic with transition temperature of 65 K for Ca, 45 K for Sr and 20 K for Ba while $A_{14}MnAs_{11}$ have no magnetic order until 5 K.[41] In the Eu-containing compounds, $Eu_{14}InPn_{11}$ compounds are paramagnetic and $Eu_{14}CdAs_{11}$ has magnetic transition at ~30 K as Cd is divalent, leaving a hole in the structure and increasing the carrier concentration.[36, 46] When Eu and Mn are in the same compound, the magnetic interactions are stronger and the transition temperatures are higher.[39, 46, 89] $Eu_{14}MnPn_{11}$ has a ferromagnetic transition of 52 K for P, 74 K for As and 100 K

for Sb. [39, 46] The saturation moments and effective moments are almost the same in $Eu_{14}MnPn_{11}$ (Pn = P, As and Sb) compounds. $Yb_{14}MnSb_{11}$ is one of the most studied compounds of the $A_{14}MPn_{11}$ analogs. X-ray magnetic circular dichroism (XMCD) shows that the $[MnSb_4]^{9-}$ tetrahedral cluster has an electronic state of $d^5 + h$ (hole) in $Yb_{14}MnSb_{11}$,[68] consistent with the theoretical calculations on $A_{14}MnBi_{11}$ described above.[54] A hole on Sb, aligned with the *d* spins on Mn^{2+}, polarizes a spin on the Sb in the $[MnSb_4]^{9-}$ cluster which screens one *d* electron leading to the description of $d^5 + h$. Therefore, $Yb_{14}MnSb_{11}$ has a saturation moment of 4 μ_B and an effective moment of 4.9 μ_B. XPS supports the model of all the Yb as 2+ in this compound.[44] The description of a partially screened electron ($d^5 + h$) model is supported by recent neutron diffraction and spectroscopy on large single crystals.[69] This model of a $[MnSb_4]^{9-}$ cluster with $d^5 + h$ is also consistent with the carrier concentration of $Yb_{14}MnSb_{11}$.[17] The Bi analogs have different magnetic properties from the other Pn atoms in that the Bi analogs have lower transition temperatures and complex transitions. For example, $Ca_{14}MnBi_{11}$, $Sr_{14}MnBi_{11}$ and $Ba_{14}MnBi_{11}$ respectively have transition temperatures of 55 K, 33 K and 15 K.[50] Although a decrease of transition temperatures are observed from Ca to Ba, the Bi compounds have lower transition temperatures than Sb compounds. Similarly, $Eu_{14}MnBi_{11}$ has a transition temperature of 35 K, lower than those of P-, As- and Sb-containing compounds mentioned above.[90] Colossal magnetoresistance behavior was discovered in $A_{14}MPn_{11}$ compounds, correlated with the magnetic ordering temperature. Magnetoresistance (MR) is defined as $MR(H) = ((\rho(H) - \rho(H=0))/ \rho(H))$ where $\rho(H)$ represents the resistivities measured with an applied field, H. The term "colossal" is employed with the MR onset correlated with the magnetic ordering temperature. The MR can be either negative or positive. While there has been a great deal of study in the detailed mechanism of other systems, such as the perovskites, the underlying mechanism for the MR observed in these compounds has not been determined. To date only negative MR has been observed in $A_{14}MPn_{11}$ systems. While that is typical for compounds with a ferromagnetic ordering temperature, it is unusual for an antiferromagnetically ordered compound to show negative MR. This is reported for $Eu_{14}MnBi_{11}$ suggesting that complex magnetic interactions are important in this compound which has two magnetic ions, Eu^{2+} and Mn^{2+}.[90]

$A_{14}MgSb_{11}$ (A = Ca, Yb) has also been prepared and studied theoretically (Figure 13).[91] Mg forms covalent bonds in the $MgSb_4$ cluster, similar to Al and Mn in $Ca_{14}AlSb_{11}$ and $Yb_{14}MnSb_{11}$. Figure 14 shows ELF distribution in the $MgSb_4$ tetrahedron with attractors corresponding to the four covalent Mg-Sb bonds. The Sb_3^{7-} unit shows a torus distribution of the ELF around each

antimony atom consistent with the 3-atom-4-electron bonding description. The ELF torus is uniform for the central Sb atom (Figures 14 C, F, and G), and has two pronounced maxima for the terminal Sb atoms (Figures 14 E and G), as expected for the bonding description.[45] These results are consistent with other theoretical descriptions of this structure type.[47, 51-54, 88] If one assumes a simple rigid band model and that Yb is 2+ in $Yb_{14}MgSb_{11}$, similar to $Yb_{14}MnSb_{11}$, an additional hole is expected. However, it is possible that Yb may exist in this structure as mixed or intermediate valence as $Yb^{2+/3+}$, as discovered in $Yb_{14}ZnSb_{11}$.[92] Magnetic measurements have been reported for $Eu_{14}MgSb_{11}$.[47] The magnetic susceptibility is similar to $Eu_{14}InBi_{11}$,[46] with a moment of 8.13 μ_B, which is close to the theoretical value of 7.937 μ_B, expected for the Eu^{2+} ion with total angular momentum J = 7/2 and the Landé g factor = 2.[47] A low temperature magnetic ordering is observed at about 7 K, consistent with the resulting value of θ of -9.49 K. Resistivity was obtained from room temperature to 900 K and gradually increases from 3.93 to 5.08 mΩ·cm, characteristic of a heavily dope semiconductor or semi-metal.[47] The $Eu_{14}MgBi_{11}$ magnetic data are reported[51] and are very similar to that of $Eu_{14}MgSb_{11}$. The compound shows antiferromagnetic ordering at 8 K, close to the obtained Weiss constant of -11.8 K. The effective moment of 8.1 μ_B is in agreement with Eu^{2+}. Resistivity from 300 – 900 K is low, staying between 2- 3 mΩ·cm, suggesting metallic behavior.[51]

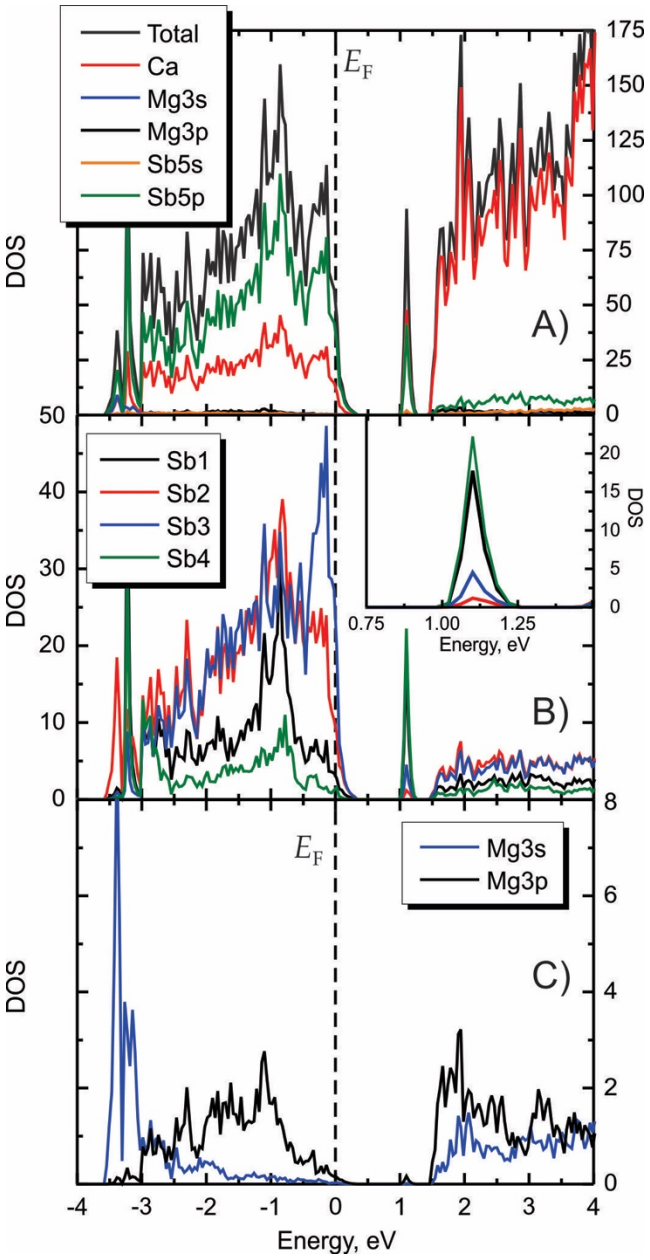

Figure 13. Density of states (DOS) diagram for $Ca_{14}MgSb_{11}$. (A) Total DOS together with partial contributions for all atoms. (B) Partial DOS showing the contributions of only Sb atoms, inset shows enlarged peak at 1.1 eV. (C) Partial DOS showing Mg atoms contributions. Reprinted with permission from [Hu, Y.; Wang, J.; Kawamura, A.; Kovnir, K.; Kauzlarich, S. M., $Yb_{14}MgSb_{11}$and $Ca_{14}MgSb_{11}$—New Mg-Containing Zintl Compounds and Their Structures, Bonding, and Thermoelectric Properties. *Chemistry of Materials* **2015,** *27*, 343-351.] Copyright 2016 by the American Chemical Society.

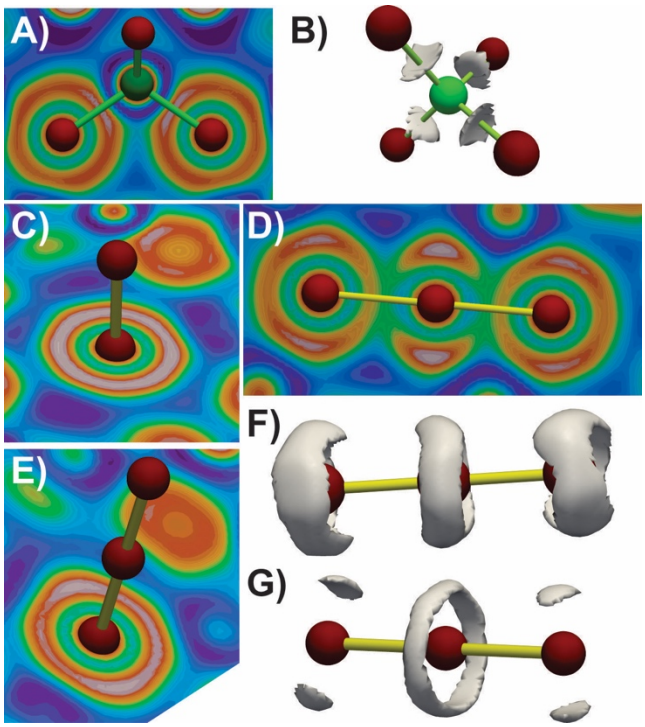

Figure 14. Coloring and 3D isosurfaces of the electron localization function (η) for $MgSb_4$ tetrahedron (B: $\eta = 0.708$) (A) and (B). Coloring (C, D, E) and 3D isosurfaces (F, G) of the ELF for Sb_3 linear unit, (F: $\eta = 0.69$; G: $\eta = 0.74$). Mg: green; Sb: red. Reprinted with permission from [Hu, Y.; Wang, J.; Kawamura, A.; Kovnir, K.; Kauzlarich, S. M., $Yb_{14}MgSb_{11}$and $Ca_{14}MgSb_{11}$—New Mg-Containing Zintl Compounds and Their Structures, Bonding, and Thermoelectric Properties. *Chemistry of Materials* **2015,** *27*, 343-351.] Copyright 2016 by the American Chemical Society.

Table 2. Reported physical properties of reported $A_{14}MPn_{11}$ compounds

Compound	Electrical	Band gap (eV)	Magnetism	*Transition Temperature (K)*	Ref
P					
$Ca_{14}MnP_{11}$	-	-	Paramagnetism	-	[38]
$Eu_{14}MnP_{11}$	Semiconductor	0.31	Ferromagnetism	52	[39]
As					
$Ca_{14}GaAs_{11}$	Semiconductor	-	-	-	[40]
$Ca_{14}MnAs_{11}$	Semiconductor	0.18	Paramagnetism	-	[41]
$Eu_{14}MnAs_{11}$	Semiconductor	0.03	Ferromagnetism	74	[39]
$Eu_{14}CdAs_{11}$	Metallic	-	Ferromagnetism	30	[36]
$Sr_{14}GaAs_{11}$	Semiconductor	-	-	-	[43]
$Sr_{14}MnAs_{11}$	Semiconductor	0.25	Paramagnetism	-	[41]
Sb					
$Yb_{14}MnSb_{11}$	Metallic	-	Ferromagnetism	53	[11, 12, 69, 93-97]
$Yb_{14}MgSb_{11}$	Metallic	-	-	-	[45]

$Yb_{14}ZnSb_{11}$	Metallic		Intermediate valence		[92]
$Ca_{14}AlSb_{11}$	Semiconductor	0.01	-	-	[48]
$Ca_{14}MnSb_{11}$	Metallic	-	Ferromagnetism	65	[41]
$Ca_{14}ZnSb_{11}$	Semiconductor	0.004	-	-	[35]
$Ca_{14}CdSb_{11}$	Semiconductor	0.08	-	-	[35]
$Ca_{14}MgSb_{11}$	Semiconductor	0.15	-	-	[45]
$Eu_{14}MnSb_{11}$	Semiconductor	-	Ferromagnetism	100	[46, 89]
$Eu_{14}MgSb_{11}$	Semi-metal	-	Antiferromagnetism	7	[47]
$Sr_{14}AlSb_{11}$	Semiconductor	0.07	-	-	[48]
$Sr_{14}MnSb_{11}$	Semiconductor	-	Ferromagnetism	45	[41]
$Sr_{14}ZnSb_{11}$	Semiconductor	0.02	-	-	[35]
$Eu_{14}InSb_{11}$	-	-	Complex	15	[46]
$Sr_{14}CdSb_{11}$	Semiconductor	0.01	-	-	[36]
$Ba_{14}AlSb_{11}$	Semiconductor	0.48	-	-	[48]
$Ba_{14}MnSb_{11}$	Semiconductor	-	Ferromagnetism	20	[41]
Bi					
$Yb_{14}MgBi_{11}$	Metallic	-	-	-	[49]
$Yb_{14}MnBi_{11}$	Metallic	-	Ferromagnetism	60	[11]
$Ca_{14}MnBi_{11}$	Metallic	-	Ferromagnetism	55	[50, 98]
$Ca_{14}MgBi_{11}$	semiconductor		-	-	[51]
$Eu_{14}InBi_{11}$	-	-	Antiferromagnetism	7	[46]
$Eu_{14}MnBi_{11}$	-	-	Complex	35	[90]
$Sr_{14}MnBi_{11}$	Metallic	-	Ferromagnetism	33	[50, 99]
$Sr_{14}MgBi_{11}$	Semi-metal	-	-	-	[51]
$Ba_{14}MnBi_{11}$	Metallic	-	Antiferromagnetism	15	[50, 99]
$Eu_{14}MgBi_{11}$	Metallic	-	Antiferromagnetism	8	[51]

Rare earth substitutions of Yb show that the specific sites affect the magnetism of $Yb_{14}MnSb_{11}$.[31] Below the ferromagnetic ordering temperature, the saturation moment for $Yb_{14-x}RE_xMnSb_{11}$ (*RE* = La, Ce, Pr, Nd and Sm, $0 < x < 0.7$) is the same as $Yb_{14}MnSb_{11}$ while in $Yb_{14-x}RE_xMnSb_{11}$ (*RE* = Gd, Tb, Dy, Ho, Er and Tm $0 < x < 0.5$) it increases with *RE* amounts.[31, 60-62, 78] This indicates that light rare earth elements are not ordered while heavy rare earth elements are ferromagnetically ordered with Mn moments. The relation between the *De Gennes* factor and transition temperature also indicates that *RE* sublattice may be involved with the magnetic interactions in $Yb_{14}MnSb_{11}$.[31] A spin re-orientation from *ab* plane to *c*-direction appearing below the transition temperatures is observed in Pr and Nd substituted samples. The spin re-orientation may explain the abnormal transition in $Yb_{14}MnBi_{11}$ below the transition temperature.[31] In any case, the complex magnetic ordering indicates that ignoring Yb and Sb sites may oversimplify the mechanism in some cases, although Mn is the only magnetic atom in $Yb_{14}MnSb_{11}$.

In the case of $Ca_{14}MnPn_{11}$ (Pn = Sb, Bi) substituted with rare earths, the magnetic data are different.[65, 66] The most striking difference for $Ca_{14-x}RE_xMnBi_{11}$ is the fact that $x_{max} = 1$. This may be attributed to the fact that they were prepared via Pb flux rather than Sn flux or is a function of

the solubility of the 3+ *RE* ion in Ca vs Yb. All of the compounds appear to be small band-gap semiconductors. Their magnetic properties are similar to the pristine compound $Ca_{14}MnPn_{11}$ as all show a ferromagnetic ordering, but at lower temperatures, dependent on the nature of the *RE* ion. Electrical resistivity is not reported for the Bi containing compounds. The Curie temperatures for the $Ca_{14-x}RE_xMnBi_{11}$ series follow the *de Gennes* scaling for *RE* = Gd–Ho, while it is proposed that short-range antiferromagnetic interactions for *RE* = Ce–Nd reduce the effect of the *RE* ion on the magnetic ordering temperature.[65] It would be useful to measure resistivity of the Bi series, along with MR for all of the $Ca_{13}REMnPn_{11}$ compounds.

3.2 Thermoelectric Properties

Thermoelectric materials, which can convert heat into electricity under a temperature gradient or vice versa, are a potential solution to the energy problem. Radioisotope Thermoelectric Generators (RTGs) for space explorations and remote power applications such as oil pipelines and deep sea detection[100, 101] and are utilized in extreme environment where photovoltaics are not suitable such as deep space or dusty environments. Compared with traditional combustion engines, thermoelectric materials have advantages in sustainability, reliability, flexibility and scalability. In order to evaluate the efficiency of thermoelectric materials, the dimensionless figure of merit (zT) represented by Equation (1) is employed:

$$zT = \frac{\alpha^2\sigma}{\kappa}T \tag{1}$$

where α represents the Seebeck coefficient ($\Delta V/\Delta T$) which is the voltage difference produced by temperature difference, σ represents the electrical conductivity, T represents the average temperature and κ represents thermal conductivity. According to Eqn(1), a high efficiency thermoelectric material should have three characteristics: a high Seebeck coefficient, a high electrical conductivity and a low thermal conductivity. The efficiency of thermoelectric devices can be related to zT values using equations below:

$$\eta_g = \frac{T_H - T_C}{T_H} \times \frac{\sqrt{1+Z\overline{T}}-1}{\sqrt{1+Z\overline{T}}+\frac{T_C}{T_H}} \tag{2}$$

$$\eta_r = \frac{T_C}{T_H - T_C} \times \frac{\sqrt{1+Z\overline{T}}-\frac{T_H}{T_C}}{\sqrt{1+Z\overline{T}}+1} \tag{3}$$

in which η_g is the efficiency of generator mode, η_r is the efficiency of refrigerator mode, T_H is the temperature of the hot end, and T_C is the temperature of the cold end. In Eqn (2), $(T_H-T_C)/T_H$ is the ideal efficiency of Carnot cycle of generator mode and in Eqn (3) $T_C/(T_H-T_C)$ is the ideal efficiency of Carnot cycle of refrigerator mode. According to these equations, the efficiency of a thermoelectric device is always smaller than the ideal Carnot cycle.

In general, materials with peak zT values above 1 are considered to be superior for thermoelectric applications and the maximum zT values reported to date is 2.6,[102] although great efforts have been made to optimize existing thermoelectric materials, discover new ones and improve average zT. The difficulty of improving zT values in thermoelectric materials lies in the fact that the three variables (Seebeck coefficient, electrical resistivity and thermal conductivity) are related to each other and more or less dependent on carrier concentration. Electrical resistivity and Seebeck coefficient (assuming a single parabolic model) can be presented by Equation (2) and (3):

$$\sigma = ne\mu \tag{2}$$

$$\alpha = \frac{8\pi^2 k_B^2}{3eh^2} m^* T \left(\frac{\pi}{3n}\right)^{\frac{2}{3}} \tag{3}$$

where n presents the carrier concentration, μ presents the carriers mobility, m^* presents the effective mass of carriers, k_B is the Boltzmann constant and h is Planck's constant. Thus, a high electrical conductivity relies on a large carrier concentration and a high carrier mobility. Meanwhile, a high Seebeck coefficient relies on a large effective mass of carriers and a small carrier concentration. The reverse effect of carrier concentrations on electrical resistivity and Seebeck coefficient requires a careful control of n to optimize thermoelectric materials and achieve high zT values. Generally speaking, semiconductors can meet the aforementioned requirements due to the ability of these materials to obtain an optimal carrier concentration and balance between Seebeck coefficient and electrical resistivity. Considering thermal conductivity, the effect of carrier concentrations will be more complex. The total thermal conductivity is the sum of electronic κ_e, lattice κ_l, and bipolar κ_b terms. Among the three terms, electronic term is related to electrical conductivity:

$$\kappa = \kappa_e + \kappa_l + \kappa_b \tag{4}$$

$$\kappa_e = L\sigma T \tag{5}$$

where L is Lorentz number. Therefore, a large carrier concentration will also increase the thermal conductivity. An optimum zT value is achieved when the carrier concentration is appropriately adjusted. The Lorentz number, Eqn(7) may vary at different temperatures and can be calculated based on Seebeck coefficient Eqn(8) as follows:

$$L = \left(\frac{k_B}{e}\right)^2 \frac{3F_0(\eta)F_2(\eta) - 4F_1(\eta)^2}{F_0(\eta)^2} \tag{7}$$

$$\alpha = \frac{k_B}{e}\left[\frac{2F_1(\eta)}{F_0(\eta)} - \eta\right] \tag{8}$$

where η is the reduced *Fermi*-level and $F_n(\eta)$ is the Fermi-Dirac integral. The *Lorentz* number for free electrons is 2.45×10^{-8} V^2/K^2. In thermoelectric materials, the *Lorentz* number is smaller than the value for free electrons and is around $1.6\text{-}1.8\times10^{-8}$ V^2/K^2 when the Seebeck coefficient is higher than 150 μV/K.

Besides adjusting the carrier concentration, another way to improve thermoelectric materials is to decrease the lattice thermal conductivity. Slack proposed a corresponding concept "Phonon Glass Electron Crystal" (PGEC),[103] which specifies that a good thermoelectric material should behave like glass to scatter phonons without significant disruption of electrons transportation. There are three ways to decrease lattice thermal conductivity. Large unit cells with heavy and numerous atoms and complex structures have intrinsically low thermal conductivity as more atoms lead to more phonon modes and stronger interactions between phonon modes.[25, 32, 104] Point defects such as vacancies, site disorders and substitutions can effectively decrease lattice thermal conductivity due to mass difference scattering. Nanostructures in the materials can add grain boundaries into the structure and scatter phonons.[105]

Several systems and structure types have been discovered to be good thermoelectric materials.[106] For instance, n- and p-type Bi_2Te_3 is a good thermoelectric material near room temperature. Materials such as SnSe, p-type TAGS, n- and p-type skutterudites and clathrates are good thermoelectrics in the medium temperature range,[102, 107-110] and n- and p-type Si-Ge alloys, n-type $La_{3-x}Te_4$ and p-type $Yb_{14}MnSb_{11}$ are good thermoelectric materials in the high temperature range.[111-113] As different materials have peak efficiency in different temperature ranges, materials can be combined sequentially to achieve an overall high efficiency for a large temperature differential. $Yb_{14}MnSb_{11}$ has a good compatibility factor for segmentation with other mid-

temperature high efficiency thermoelectric materials[17] leading to an unprecedented 11-15% efficiency demonstration in a segmented thermoelectric device.[114]

The thermoelectric properties of a variety of *Zintl* phases have been recently reviewed.[26, 27, 32] As a *Zintl* phase compound, $Yb_{14}MnSb_{11}$ (Fig. 1) is a typical example of PGEC concept.[111, 115] The large unit cell, complex structure and large number of atoms in the unit cell lead to intrinsically low lattice thermal conductivity. It is the best *p*-type thermoelectric material in the high temperature region so far (800-1275 K) and has a zT value of ~1.2 at 1275 K, doubling the efficiency of previous Si-Ge alloys and is currently being developed by NASA for high temperature radioisotope thermoelectric generators.[116]

The preparation methodologies of $Yb_{14}MnSb_{11}$ can significantly affect the thermoelectric properties. Powder metallurgy method provides $Yb_{14}MnSb_{11}$ with a higher zT value (~1.2 at 1275 K) than the single crystal sample prepared by Sn-flux method (~1.0 at 1275 K).[111, 117] The difference in unit cell parameters provides some clues. There may be Yb or Mn defects (slight sub-stoichiometry) in the samples prepared by Sn-flux method, leading to a smaller unit cell and higher p-type carrier concentration for those samples. These defects, while having only a minor effect on the electrical resistivity and the thermal conductivity, dramatically decrease the Seebeck coefficient. Standard single crystal X-ray diffraction does not provide evidence for non-stoichiometry, but the changes in unit cell as a function of preparation method are a good indication. The net effect is a significant decrease of zT values for samples prepared via Sn flux or for sub-stoichiometric phases. Other properties of $Yb_{14}MnSb_{11}$ have also been measured such as evaporation and thermal expansion.[118, 119]

To optimize thermoelectric properties of $Yb_{14}MnSb_{11}$, several studies have been carried out by employing solid solutions of various substituents.[59, 63, 76, 82, 85, 86, 120] The reported literature data can be analyzed using the well-established single parabolic band (SPB) model.[121] It is utilized here to examine the impact of compositional changes (i.e. alloying/doping) on the experimental density of states effective mass, m^*_{DOS} and to assess the impact to the electronic transport. The majority of the reported thermoelectric properties are centered on $Yb_{14}MnSb_{11}$ analogues with substitutions on one of the three elemental positions in order to improve upon the already high zT. For example, rare earth (*RE*) to tune the carrier concentration or alkaline earth (*AE*) doping on the Yb position to reduce the thermal conductivity, Mg/Al/Zn doping on the Mn position to tune the carrier concentration and reduce the spin disorder scattering, Te/Bi alloying on the Sb site to

change the carrier concertation and/or band gap. Due to the limited amount of high temperature data reported in literature, the analysis of the data using the SPB model is limited to 300 K. A comparison at higher temperatures would have been useful to provide a more general picture, but we would have lost a significant amount of data. Figure 15 shows Hall mobility (a) and Seebeck (b) as a function of the Hall carrier concentration for the reported $A_{14}MPn_{11}$ compounds at 300 K. The data can be modeled using $m^*_{DOS} \sim 1.8\ m_e$ on the lower limit with the upper limit being and $m^*_{DOS} \sim 3.0\ m_e$. The model assumes that acoustic phonon scattering is the dominant scattering mechanism, however other scattering mechanisms such as grain boundary[122] and ionized impurity scattering or impurities in the samples could also contribute and lead to spread in the data set. After examination of the data with the SPB model, a few trends are apparent: when trivalent rare earth elements substitute Yb, one electron is donated to the structure which decreases the carrier (holes) concentration. On the Yb site, trivalent rare earth (*RE*) elements are found to form limited solid solutions (less than 5%) whereas alkaline earths such as Ca form a full solid solution.[59, 63, 76, 120] Substitution of Ca has a similar effect as the substitution of a RE^{3+} ion in that it lowers the carrier concentration. While many papers cite the fact that Ca is more electropositive than Yb and can transfer electrons more completely to the anions, it is more likely that Ca reduces the amount of defect in the compound since both Yb and Ca are divalent.[123] $Yb_{14-x}Ca_xMnSb_{11}$ (x = 1, 2, 4, 6, 8) was found to decrease the density of material effectively and showed slightly larger zT values, which may help in practical applications where the cost of the rare earth and mass are of concern. However, substitution of Yb with Ca makes the compound more air-sensitive and the best x value that gives rise to good transport properties without too much air-sensitivity was found to be 4.[75] When early *RE* elements such as La, Ce, Pr, Sm dope on the Yb site, they tend to have lower mobilities and slightly higher Seebeck coefficients when compared to the $Yb_{14}MnSb_{11}$ system and the data can be fit using a lower effective mass ~1.8 m_e. The changes of properties are not linear with the substitution amount, indicating that *f*-levels of *RE* may have significant effects around Fermi-level. The changes are likely due to movement of the Fermi level lower into the valence band due to the influence of the *f*-electron states in the rare earths and from the bonding states of the *RE*-Pn sites. However, when late *RE* such as Lu is doped, the carrier concentration and mobility trends are relatively flat and seem to shift to the higher effective mass. This may be attributed to the filled *f*-orbital (f^{14}) for both Lu^{3+} and Yb^{2+}.

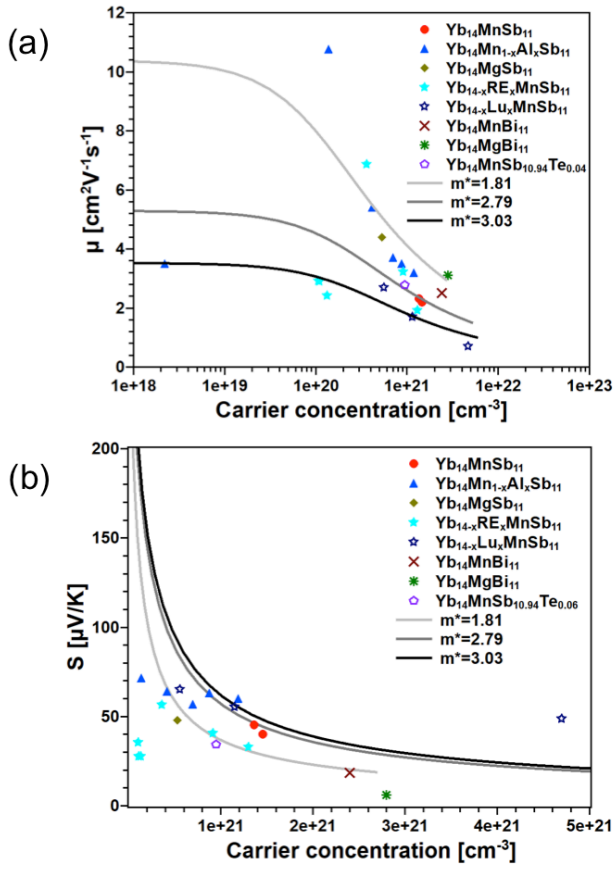

Figure 15. a) Mobility and b) Seebeck as function of carrier concentration for $Yb_{14}MnSb_{11}$ analogues at 300 K.

The data on doping on the Pn site are limited to Ge, Te, and Sn which only substitute for a trace amount of Sb in the structure.[85-87] However, Bi has been shown to make a full isoelectronic solid solution.[84, 124] The doping of the Sb site with Ge, Te, or Bi differently affects the carrier concentration (higher for Bi and lower for Te, the same for Ge), but in all cases leads to an increased mobility which correspond to a lower effective mass. This may be attributed to the large contributions of Sb orbitals to the bands just below the Fermi-level. The Sb3 site has the largest contribution and it is the isolated Sb^{3-} site, which is the easiest to be substituted. From the density of states calculations, it is found that the Sb sites contribute to the band gap of the material. Thus, alloying with heavy elements such as Bi could reduce the band gap and move the Fermi level deeper in the valence band.

Alloying on the Mn with 3+ or 2+ metals such as Mg, Zn, or Al has a significant impact on the thermoelectric transport. Alloying with Al^{3+} provides additional electrons to the system moving it towards the charge balanced *Zintl* composition. It leads to reduced carrier concentrations, higher mobilities and higher Seebeck coefficients. The data for $Yb_{14}AlSb_{11}$ can be fit with a higher effective mass ~2.7-3.0 m_e, indicating a transition to a heavier band. It should be noted that Al alloying which was investigated very early on shows significant changes in the doping range as well as for the effective mass. The fully substituted $Yb_{14}MgSb_{11}$ analogue also seems to track with a higher effective mass; however, more data are needed to establish trends. The significant change in the transport properties as a result of alloying/doping on the M site is reasonable, considering the previously discussed band structure calculations, which shows that the valence band edge is dominated by the M-Pn sites (Figures 11 & 13). Therefore, it is not surprising that the identity of the M site would have a significant impact on the thermoelectric transport properties.

It is well established that the thermal conductivity of the $Yb_{14}MnSb_{11}$ structure is relatively low when compared to other state of the art thermoelectric materials such as SiGe, PbTe and $CoSb_3$.[104] This inherently low thermal conductivity is attributed to the structural complexity of the material, the large unit cell composed of heavy atoms, and due to a significant scattering of the low lying optical modes in the phonon density of states. The minimum lattice thermal conductivity, κ_l, also known as the glassy limit, of the $Yb_{14}MnSb_{11}$ was previously calculated using the Cahill approximation to be 0.4 W/mK.[124] The lattice thermal conductivity of the reported $Yb_{14}MPn_{11}$ compounds was calculated using the previously defined relations in equation 5 and 6. The total thermal conductivity, κ_t, was extracted from published data. It should be noted that different values of heat capacity were utilized in the various literature reports and this variance in the heat capacity could result in up to 20-30% differences in the κ_t values. Figure 16 compares the calculated κ_l for the $Yb_{14}MPn_{11}$ variants with the glassy minimum of 0.4 W/mK at 300 K. All the materials show similar and low lattice thermal conductivities, with the highest thermal conductivity attributed to $Yb_{14}MnSb_{11}$, implying that substitution and alloying with other elements leads to a reduction in the lattice thermal conductivity. This reduction in κ_l may be due to point-defect scattering/alloy scattering of the phonons. The $Yb_{14}MPn_{11}$ compounds are considerably higher than the glassy minimum at 300 K. $Yb_{14}ZnSb_{11}$ appears to have anomalously low lattice thermal conductivity, this may be due to a failure of the Wiedemann-Franz limit and over estimation of L due to the metallic nature of the Zn system.[125]

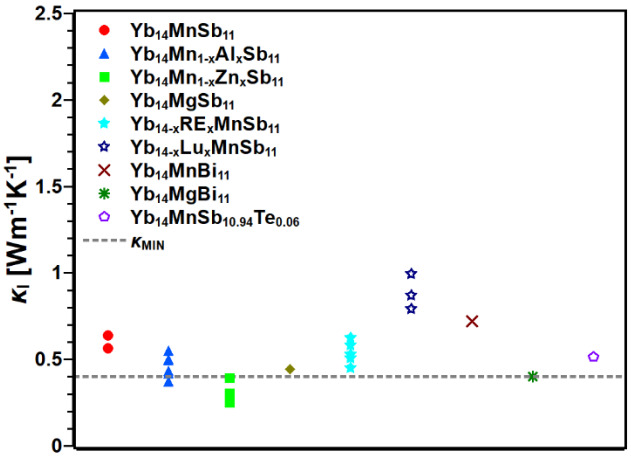

Figure 16. Lattice thermal conductivities vs composition for $Yb_{14}MnSb_{11}$ analogues. The glassy limit of κ_l is shown in grey.

Figure 17 compares the *zT*s of the $A_{14}MPn_{11}$ materials with that of the predicted *zT*s from the SPB model at 300 K. For simplicity, the lattice thermal conductivity for the m^*_{DOS} 2.7 and 3.0 bands is fixed to the lattice thermal conductivity of the $Yb_{14}MnSb_{11}$ (0.8 W/mK). The model is in relatively good agreement with the calculated *zT* from experimentally obtained values. The deviation in the data can be attributed to other scattering mechanisms that are not captured by the SPB (grain boundary/impurity scattering), or to measurement errors. It is also possible that the SPB model does not adequately account for changes due to structure distortions, defects, site preferences, and orbital interactions of the various alloy elements. Another approach often found in literature is represented by the so-called Jonker's plot, where logS is plotted against logσ. In this way, the dependence from the charge carrier concentration is eliminated along with the error in the measurement of *n* arising from the low Hall signal characteristic of materials with high carrier density. However, we decided not to show the Jonker's plot, because at high doping levels and at low temperatures it is affected by uncertainty caused by impurity conduction,[126] while at high temperature we could have shown only a limited amount of data, which would have limited the plot to only a few systems.

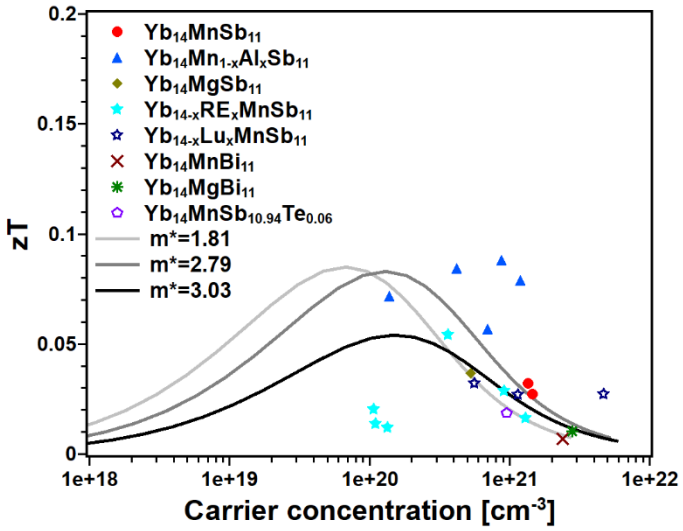

Figure 17. *zT* as predicted by the SPB model vs carrier concentration.

3.3 Summary and Future Directions

This review summarizes much of the current progress in structure –property investigations of Zintl phases with the $Ca_{14}AlSb_{11}$ structure type, providing a foundation for future directions. The potential for significant new discoveries of novel magnetics and thermoelectric properties is great. Although a number of analogs of $Ca_{14}AlSb_{11}$ have been investigated, there are many new analogs to be discovered and studied. In addition, some compositions are not completely characterized by transport, magnetoresistance and detailed magnetic studies. Further optimization of existing alloy phases is also possible as the structure type is highly flexible for solid solutions and dopants. Optimization of the $Yb_{14}MnSb_{11}$ system may require doping on all sites, as all sites play a critical role in the thermoelectric transport. More high level theoretical calculations could add in focusing on the most promising systems. The solid solution of $Yb_{14}Mn_{1-x}Al_xSb_{11}$ has shown the greatest promise with regard to changes in the band structure whereas alloying with *RE* may assist in tuning of the carrier concentration to the optimum level. Alloying with heavier elements such as Bi could be utilized to reduce the band gap and optimize the *zT* for various temperature ranges. As more analogs of this structure type are discovered and characterized, there is a high likelihood for significant potential for these compounds and other Zintl phases to provide technologically relevant properties.

Acknowledgements:

SMK thanks past post-docs, graduate and undergraduate students who have contributed to this work along with current and past members of the JPL Advanced ThermOelectric Materials (ATOM) group for insight and useful discussion. Much of this work was funded by NSF, most recently DMR-1709382. This research has also benefitted financially from DOE-NEUP. Part of this work was performed at the California Institute of Technology/Jet Propulsion Laboratory under contract with the National Aeronautics and Space Administration. This work was supported by the NASA Science Missions Directorate under the Radioisotope Power Systems Program. GC's research at Jet Propulsion Laboratory is supported by an appointment to the NASA Postdoctoral Program, administered by Universities Space Research Association (USRA) under contract with NASA.

References

1. Schäfer, H.; Eisenmann, B.; Müller, W., Zintl Phases : Transitions between Metallic and Ionic Bonding. *Angew. Chem. internat. Ed.* **1973,** *12*, 694-712.
2. Kauzlarich, S. M., *Chemistry, Structure, and Bonding of Zintl Phases and Ions*. VCH Publishers, Inc: New York, 1996.
3. Deller, K.; Eisenmann, B., On the Intermetallic Compounds $Ca_{11}Sb_{10}$ and $Ca_{11}Bi_{10}$. *Z. Naturforsch.* **1976,** *31b*, 29-34.
4. Queneau, V.; Sevov, S. C., Synthesis and Structure of the Zintl-Phase K_4Pb_9 Containing Isolated Pb_9^{4-} Clusters of Two Different Geometries. *Inorg. Chem.* **1998,** *37*, 1358-1360.
5. Kasper, J. S.; Hagenmuller, P.; Pouchard, M.; Cros, C., Clathrate Structure of Silicon Na_8Si_{46} and Na_xSi_{136} (x < 11). *Science (Washington, DC, U.S.)* **1965,** *150*, 1713–1714.
6. Cordier, G.; Schäfer, H.; Stelter, M., Darstellung und Struktur der Verbindung $Ca_{14}AlSb_{11}$. *Zeitschrift fuer Anorganische und Allgemeine Chemie* **1984,** *519*, 183-188.
7. Gascoin, F.; Sevov, S. C., KBa_2InAs_3 with Coexisting Monomers of $[In_2As_7]^{13-}$ and Their One-Dimensional Polymers. *Inorg. Chem.* **2002,** *41*, 2292-2295.
8. Kauzlarich, S. M., Transition Metal Zintl Compounds. In *Chemistry, Structure, and Bonding of Zintl Phases and Ions*, Kauzlarich, S. M., Ed. VCH Publishers, Inc.: New York, 1996; pp 245-274.
9. Kauzlarich, S. M., A rational approach to solid state synthesis-the Zintl concept. *Comment Inorganic Chem* **1990,** *10*, 75-88.
10. Kauzlarich, S. M.; Payne, A. C.; Webb, D. J., Magnetism and Magnetotransport Properties of Transition Metal Zintl Isotypes. In *Magnetism: Molecules to Materials III*, Miller, J. S.; Drillon, M., Eds. Wiley-VCH: Weinham, 2002; pp 37-62.
11. Chan, J. Y.; Olmstead, M. M.; Kauzlarich, S. M.; Webb, D. J., Structure and Ferromagnetism of the Rare-Earth Zintl Compounds: $Yb_{14}MnSb_{11}$ and $Yb_{14}MnBi_{11}$. *Chemistry of Materials* **1998,** *10*, 3583-3588.
12. Fisher, I. R.; Wiener, T. A.; Bud'ko, S. L.; Canfield, P. C.; Chan, J. Y.; Kauzlarich, S. M., Thermodynamic and transport properties of single-crystal $Yb_{14}MnSb_{11}$. *Physical Review B: Condensed Matter and Materials Physics* **1999,** *59*, 13829-13834.
13. Chen, X.; Shen, J. N.; Wu, L. M.; Chen, L., A ferrimagnetic Zintl phase Pr_4MnSb_9: synthesis, structure, and physical properties. *Inorganic chemistry* **2013,** *52*, 7441-7447.
14. Holm, A. P.; Olmstead, M. M.; Kauzlarich, S. M., The Crystal Structure and Magnetic Properties of a New Ferrimagnetic Semiconductor: $Ca_{21}Mn_4Sb_{18}$. *Inorganic Chemistry* **2003,** *42*, 1973-1981.
15. Bobev, S.; Thompson, J. D.; Sarrao, J. L.; Olmstead, M. M.; Hope, H.; Kauzlarich, S. M., Probing the Limits of the Zintl Concept: Structure and Bonding in Rare-Earth and Alkaline-Earth Zinc-Antimonides $Yb_9Zn_{4+x}Sb_9$ and $Ca_9Zn_{4.5}Sb_9$. *Inorganic Chemistry* **2004,** *43*, 5044-5052.

16. Gascoin, F.; Sevov, S. C., Ternary and Quaternary Niobium Arsenide Zintl Phases. In *Inorganic chemistry in focus: III*, Meyer, G.; Naumann, D.; Wesemann, L., Eds. Wiley-VCH: 2006; pp 195-206.
17. Brown, S. R.; Kauzlarich, S. M.; Gascoin, F.; Snyder, G. J., $Yb_{14}MnSb_{11}$: New High Efficiency Thermoelectric Material for Power Generation. *Chemistry of Materials* **2006,** *18*, 1873-1877.
18. Ohno, S.; Zevalkink, A.; Takagiwa, Y.; Bux, S. K.; Snyder, G. J., Thermoelectric properties of the $Yb_9Mn_{4.2-x}Zn_xSb_9$ solid solutions. *Journal of Materials Chemistry A* **2014,** *2*, 7478-7483.
19. Miller, G. J.; Schmidt, M. W.; Wang, F.; You, T.-S., Quantitative Advances in the Zintl-Klemm Formalism. In *Zintl Phases: Principles and Recent Developments*, Fassler, T. F., Ed. Springer-Verlag: Berlin, 2011; Vol. 139, pp 1-55.
20. Kauzlarich, S. M.; Chan, J. Y.; Taylor, B. R., Exploitation of Zintl Phases in the Pursuit of Novel Magnetic and Electronic Materials. In *Inorganic Materials Synthesis*, Winter, C. H.; Hoffman, D. M., Eds. American Chemical Society: Washington D.C., 1999; Vol. ACS Symposium Series Vol. 727, pp 15-27.
21. Clark, H. L.; Simpson, H. D.; Steinfink, H., Crystal structure of $Yb_{11}Sb_{10}$. *Inorganic Chemistry* **1970,** *9*, 1962-4.
22. Holm, A. P.; Park, S. M.; Condron, C. L.; Olmstead, M. M.; Kim, H.; Klavins, P.; Grandjean, F.; Hermann, R. P.; Long, G. J.; Kanatzidis, M. G.; Kauzlarich, S. M.; Kim, S. J., $Eu_{10}Mn_6Sb_{13}$: A new ternary rare-earth transition-metal Zintl phase. *Inorganic Chemistry* **2003,** *42*, 4660-4557.
23. Kim, S.-J.; Salvador, J.; Bilc, D.; Mahanti, S. D.; Kanatzidis, M. G., $Yb_9Zn_4Bi_9$: Extension of the Zintl Concept to the Mixed-Valent Spectator Cations. *Journal of the American Chemical Society* **2001,** *123*, 12704-12705.
24. Gascoin, F.; Sevov, S. C., Synthesis and Characterization of Transition-Metal Zintl Phases: $Cs_{24}Nb_2In_{12}As_{18}$ and $Cs_{13}Nb_2In_6As_{10}$ with Isolated Complex Anions. *Inorganic Chemistry* **2003,** *42*, 85567-8571.
25. Toberer, E. S.; May, A. F.; Snyder, G. J., Zintl Chemistry for Designing High Efficiency Thermoelectric Materials. *Chemistry of Materials* **2010,** *22*, 624-634.
26. Shi, X.; Chen, L.; Uher, C., Recent advances in high-performance bulk thermoelectric materials. *International Materials Reviews* **2016,** *61*, 379-415.
27. Shuai, J.; Mao, J.; Song, S.; Zhang, Q.; Chen, G.; Ren, Z., Recent progress and future challenges on thermoelectric Zintl materials. *Materials Today Physics* **2017,** *1*, 74-95.
28. Nesper, R., Structure and Chemical bonding in Zintl-phases containing Li. *Prog. Sol. State Chem.* **1990,** *20*, 1-45.
29. Nesper, R., The Zintl-Klemm Concept – A Historical Survey. *Zeitschrift für anorganische und allgemeine Chemie* **2014,** *640*, 2639-2648.
30. Kauzarich, S. M., Zintl Phases with d-Metal. In *Comprehensive Inorganic Chemistry II*, 2nd ed.; Reedijk, J.; Poeppelmeier, K., Eds. Elsevier: Amsterdam, 2013; Vol. 2, pp 103-110.
31. Hu, Y.; Chen, C. W.; Cao, H.; Makhmudov, F.; Grebenkemper, J. H.; Abdusalyamova, M. N.; Morosan, E.; Kauzlarich, S. M., Tuning Magnetism of $[MnSb_4]^{(9-)}$ Cluster in $Yb_{14}MnSb_{11}$ through Chemical Substitutions on Yb Sites: Appearance and Disappearance of Spin Reorientation. *Journal of the American Chemical Society* **2016,** *138*, 12422-31.
32. Kazem, N.; Kauzlarich, S. M., Thermoelectric Properties of Zintl Antimonides. In *Handbook on the Physics and Chemistry of Rare Earths*, Elsevier: 2016; Vol. 50, pp 177-208.
33. Kastbjerg, S.; Uvarov, C. A.; Kauzlarich, S. M.; Chen, Y. S.; Nishibori, E.; Spackman, M. A.; Iversen, B. B., Crystal structure and chemical bonding of the intermetallic Zintl phase $Yb_{11}AlSb_9$. *Dalton transactions* **2012,** *41*, 10347-53.
34. Mantina M.; Valero R.; Cramer C. J.; Truhlar D. G., Atomic Radii of the Elements. In *CRC handbook of Chemistry and Physics*, 94 ed.; Haynes, W. M., Ed. CRC Press: London, 2013.
35. Young, D. M.; Torardi, C. C.; Olmstead, M. M.; Kauzlarich, S. M., Exploring the limits of the Zintl concept for the $A_{14}MPn_{11}$ structure type with M = Zn, Cd. *Chemistry of Materials* **1995,** *7*, 93-101.

36. Makongo, J. P. A.; Darone, G. M.; Xia, S. Q.; Bobev, S., Non-stoichiometric compositions arising from synergistic electronic and size effects. Synthesis, crystal chemistry and electronic properties of $A_{(14)}Cd_{(1+x)}Pn_{(11)}$ compounds (0 <= x <= 0.3; A = Sr, Eu; Pn = As, Sb). *Journal of Materials Chemistry C* **2015,** *3*, 10388-10400.
37. Vaughey, J. T.; Corbett, J. D., Synthesis and Structure of $Ca_{14}GaP_{11}$ with the New Hypervalent P_3^{7-} Anion. Matrix Effects within the Family of Isostructural Alkaline-Earth Metal Pnictides. *Chemistry of Materials* **1996,** *8*, 671-675.
38. Kim, H.; Kauzlarich, S. M., Structure and magnetic properties of $Ca_{14}MnP_{11}$. *Journal of Solid State Chemistry* **2005,** *178*, 1935-1939.
39. Payne, A. C.; Olmstead, M. M.; Kauzlarich, S. M.; Webb, D. J., Structure, magnetism, and magnetoresistance of the compounds $Eu_{14}MnAs_{11}$ and $Eu_{14}MnP_{11}$. *Chemistry of Materials* **2001,** *13*, 1398-1406.
40. Kauzlarich, S. M.; Thomas, M. M.; Odink, D. A.; Olmstead, M. M., $Ca_{14}GaAs_{11}$ - a new compound containing discrete $GaAs_4$ tetrahedra and a hypervalent As_3 polyatomic unit. *Journal of the American Chemical Society* **1991,** *113*, 7205-7208.
41. Rehr, A.; Kuromoto, T. Y.; Kauzlarich, S. M.; Del Castillo, J.; Webb, D. J., Structure and properties of the transition-metal Zintl compounds $A_{14}MnPn_{11}$ (A = Ca, Sr, Ba; Pn = As, Sb). *Chemistry of Materials* **1994,** *6*, 93-99.
42. Vidyasagar, K.; Honle, W.; von Schnering, H. G., Sr13NbAs11 and Eu13NbAs11 - Defect Variants fo the $Ca_{14}AlSb_{11}$ Structure with Asymmetric $[As_3]^{7-}$ Anions. *Z. Anorg. Allg. Chem.* **1996,** *622*, 518-524.
43. Kauzlarich, S. M.; Kuromoto, T. Y., Exploring the Structure and bonding of the Zintl compounds - $A_{14}GaAs_{11}$ (A = Ca, Sr). *Croatica Chemica Acta* **1991,** *64*, 343-352.
44. Holm, A. P.; Ozawa, T. C.; Kauzlarich, S. M.; Morton, S. A.; Dan Waddill, G.; Tobin, J. G., X-ray photoelectron spectroscopy studies of $Yb_{14}MnSb_{11}$ and $Yb_{14}ZnSb_{11}$. *Journal of Solid State Chemistry* **2005,** *178*, 262-269.
45. Hu, Y.; Wang, J.; Kawamura, A.; Kovnir, K.; Kauzlarich, S. M., $Yb_{14}MgSb_{11}$ and $Ca_{14}MgSb_{11}$—New Mg-Containing Zintl Compounds and Their Structures, Bonding, and Thermoelectric Properties. *Chemistry of Materials* **2015,** *27*, 343-351.
46. Chan, J. Y.; Wang, M. E.; Rehr, A.; Kauzlarich, S. M.; Webb, D. J., Synthesis, Structure, and Magnetic Properties of the Rare-Earth Zintl Compounds $Eu_{14}MnPn_{11}$ and $Eu_{14}InPn_{11}$ (Pn = Sb, Bi). *Chemistry of Materials.* **1997,** *9*, 2131 - 2138.
47. Tan, W. J.; Liu, Y. T.; Zhu, M.; Zhu, T. J.; Zhao, X. B.; Tao, X. T.; Xia, S. Q., Structure, Magnetism, and Thermoelectric Properties of Magnesium-Containing Antimonide Zintl Phases $Sr_{14}MgSb_{11}$ and $Eu_{14}MgSb_{11}$. *Inorganic chemistry* **2017,** *56*, 1646-1654.
48. Brock, S. L.; Weston, L. J.; Olmstead, M. M.; Kauzlarich, S. M., Synthesis, structure, and properties of $A_{14}AlSb_{11}$ (A= Ca, Sr, Ba). *Journal of Solid State Chemistry* **1993,** *107*, 513-23.
49. Hu, Y.; Kauzlarich, S. M., $Yb_{14}MgBi_{11}$: structure, thermoelectric properties and the effect of the structure on low lattice thermal conductivity. *Dalton transactions* **2017,** *46*, 3996-4003.
50. Kuromoto, T. Y.; Kauzlarich, S. M.; Webb, D. J., Structure and Properties of the Transition-Metal Zintl compounds - $A_{14}MnBi_{11}$ (A = Ca, Sr, Ba). *Chemistry of Materials* **1992,** *4*, 435-440.
51. Tan, W.; Wu, Z.; Zhu, M.; Shen, J.; Zhu, T.; Zhao, X.; Huang, B.; Tao, X. T.; Xia, S. Q., $A_{14}MgBi_{11}$ (A = Ca, Sr, Eu): Magnesium Bismuth Based Zintl Phases as Potential Thermoelectric Materials. *Inorganic chemistry* **2017,** *56*, 10576-10583.
52. Gallup, R. F.; Fong, C. Y.; Kauzlarich, S. M., Bonding properties of $Ca_{14}GaAs_{11}$ - a compound containing discrete $GaAs_4$ tetrahedra and a hypervalent As_3 polyatomic unit. *Inorganic Chemistry* **1992,** *31*, 115-118.
53. Gallup, R. F.; Fong, C. Y.; Kauzlarich, S. M., minor correction to theory paper. *Inorganic Chemistry* **1992,** *31*, 2294.

54. Sánchez-Portal, D.; Martin, R. M.; Kauzlarich, S. M.; Pickett, W. E., Bonding, moment formation, and magnetic interactions in $Ca_{14}MnBi_{11}$ and $Ba_{14}MnBi_{11}$. *Physical Review B* **2002,** *65*, 144414.
55. Carrillo-Cabrera, W.; Somer, M.; Peters, K.; Schnering, H. G. v., Synthesis, Structure and Vibrational Spectra of Ba141nP11. *Chem. Ber.* **1996,** *129*, 1015-1023.
56. Ratai, E.; Bruins, P.; Hernandez, C. J.; Kauzlarich, S. M.; Augustine, M. P., Magnetic resonance study of a series of phosphorus-containing Zintl compounds: $Ca_{14}AlP_{11}$, $Ca_{14}MnP_{11}$, and $Eu_{14}MnP_{11}$. *Chemistry of Materials* **2002,** *14*, 2467-2475.
57. Hermann, R. P.; Grandjean, F.; Kauzlarich, S. M.; Jiang, J.; Brown, S.; Long, G. J., A europium-151 Mössbauer spectral study of $Eu_{14}MnP_{11}$, $Eu_{14}MnAs_{11}$, and $Eu_{14}MnSb_{11}$. *Inorganic Chemistry* **2004,** *43*, 7005-7013.
58. Munzarová, M. L.; Hoffmann, R., Electron-Rich Three-Center Bonding: Role of s,p Interactions across the p-Block. *J. Am. Chem. Soc.* **2002,** *124*, 4787-4795.
59. Toberer, E. S.; Brown, S. R.; Ikeda, T.; Kauzlarich, S. M.; Jeffrey Snyder, G., High thermoelectric efficiency in lanthanum doped $Yb_{14}MnSb_{11}$. *Applied Physics Letters* **2008,** *93*, 062110.
60. Roudebush, J. H.; Grebenkemper, J.; Hu, Y.; Kazem, N.; Abdusalyamova, M. N.; Kauzlarich, S. M., $Yb_{14-x}Tm_xMnSb_{11}$ (0<x<0.5): Structure and magnetic properties. *Journal of Solid State Chemistry* **2014,** *211*, 206-211.
61. Grebenkemper, J. H.; Kauzlarich, S. M., Magnetic and structural effects of partial Ce substitution in Y $b_{14}MnSb_{11}$. *APL Materials* **2015,** *3*, 041503.
62. Grebenkemper, J. H.; Hu, Y.; Abdusalyamova, M. N.; Makhmudov, F. A.; Kauzlarich, S. M., Magnetic remanence in $Yb_{14-x}RE_xMnSb_{11}$ (RE=Tb, Dy, Ho) single crystals. *Journal of Solid State Chemistry* **2016,** *238*, 321-326.
63. Grebenkemper, J. H.; Klemenz, S.; Albert, B.; Bux, S. K.; Kauzlarich, S. M., Effects of Sc and Y substitution on the structure and thermoelectric properties of $Yb_{14}MnSb_{11}$. *Journal of Solid State Chemistry* **2016,** *242*, 55-61.
64. Vasilyeva, I. G.; Nikolaev, R. E.; Abdusaljamova, M. N.; Kauzlarich, S. M., Thermochemistry study and improved thermal stability of $Yb_{14}MnSb_{11}$ alloyed by Ln^{3+}(La–Lu). *J. Mater. Chem. C* **2016,** *4*, 3342-3348.
65. Ovchinnikov, A.; Prakash, J.; Bobev, S., Crystal chemistry and magnetic properties of the solid solutions $Ca_{14-x}RE_xMnBi_{11}$ (RE = La-Nd, Sm, and Gd-Ho; x approximately 0.6-0.8). *Dalton transactions* **2017,** *46*, 16041-16049.
66. Prakash, J.; Stoyko, S.; Voss, L.; Bobev, S., On the Extended Series of Quaternary Zintl Phases $Ca_{13}REMnSb_{11}$ (RE = La-Nd, Sm, Gd-Dy). *European Journal of Inorganic Chemistry* **2016,** *2016*, 2912-2922.
67. Nam, G.; Jang, E.; Jo, H.; Han, M. K.; Kim, S. J.; Ok, K. M.; You, T. S., Cationic Site-Preference in the $Yb_{14-x}Ca_xAlSb_{11}$ ($4.81 \leqslant x \leqslant 10.57$) Series: Theoretical and Experimental Studies. *Materials (Basel)* **2016,** *9*, 553.
68. Holm, A. P.; Kauzlarich, S. M.; Morton, S. A.; Waddill, G. D.; Pickett, W. E.; Tobin, J. G., XMCD Characterization of the Ferromagnetic State of $Yb_{14}MnSb_{11}$. *Journal of the American Chemical Society* **2002,** *124*, 9894-9898.
69. Stone, M. B.; Garlea, V. O.; Gillon, B.; Cousson, A.; Christianson, A. D.; Lumsden, M. D.; Nagler, S. E.; Mandrus, D.; Sales, B. C., Excitations and magnetization density distribution in the dilute ferromagnetic semiconductor $Yb_{14}MnSb_{11}$. *Physical Review B* **2017,** *95*, 020412(R).
70. Del Castillo, J.; Webb, D. J.; Kauzlarich, S. M.; Kuromoto, T. Y., Pressure-induced ferromagnetic states in $Sr_{14}MnAs_{11}$. *Physical Review B* **1993,** *47*, 4849-52.
71. Wang, Y.; Bobev, S., Synthesis and Structural Characterization of $Ca_{14}Nb_xIn_{1-x}As_{11}$, ($x \approx 0.85$). *Solid State Phenomena* **2016,** *257*, 147-151.

72. Kim, H.; Chan, J. Y.; Olmstead, M. M.; Klavins, P.; Webb, D. J.; Kauzlarich, S. M., Magnetism and colossal magnetoresistance of the pseudo-ternary rare-earth transition-metal compounds, $Eu_{14-x}Ca_xMnSb_{11}$ (x < 3). *Chemistry of Materials* **2002,** *14*, 206-216.
73. Kim, H.; Klavins, P.; Kauzlarich, S. M., Structure, magnetism, and magnetoresistance of the rare-earth transition metal compounds $Eu_{13}AMnSb_{11}$ (A = Ca, Sr, Ba, and Yb). *Chemistry of Materials* **2002,** *14*, 2308-2316.
74. Kim, H.; Olmstead, M. M.; Klavins, P.; Webb, D. J.; Kauzlarich, S. M., Structure, Magnetism, and Colossal Magnetoresistance (CMR) of the Ternary Transition Metal Solid Solution $Ca_{14-x}Eu_xMnSb_{11}$ (0 < x < 14). *Chem. Mater.* **2002,** *14*, 3382-3390.
75. Cox, C. A.; Brown, S. R.; Snyder, G. J.; Kauzlarich, S. M., Effect of Ca Doping on the Thermoelectric Performance of $Yb_{(14)}MnSb_{(11)}$. *Journal of Electronic Materials* **2010,** *39*, 1373-1375.
76. Uvarov, C. A.; Ortega-Alvarez, F.; Kauzlarich, S. M., Enhanced high-temperature thermoelectric performance of $Yb_{(14-x)}Ca_{(x)}MnSb_{11}$. *Inorganic Chemistry* **2012,** *51*, 7617-24.
77. Uvarov, C. A.; Rauscher, J. F.; Kauzlarich, S. M., High Temperature Thermoelectric Properties of $Yb_{(14-x)}Ca_{(x)}MnSb_{(11)}$ Made by Reaction of the Elements. *Science of Advanced Materials* **2011,** *3*, 646-651.
78. Sales, B. C.; Khalifah, P.; Enck, T. P.; Nagler, E. J.; Sykora, R. E.; Jin, R.; Mandrus, D., Kondo lattice behavior in the ordered dilute magnetic semiconductor $Yb_{14-x}La_xMnSb_{11}$. *Physical Review B* **2005,** *72*, 205207.
79. Abdusalyamova, M.; Vasilyeva, I., Some Physicochemical Properties of Yb14MnSb11 and Its Solid Solutions with Gadolinium $Yb_{14-x}Gd_xMnSb_{11}$ Type. In *2016 4th International Conference on Nano and Materials Science*, Yuan, Y.; Menon, L.; Xu, X., Eds. 2016; Vol. 43.
80. Vasilyeva, I.; Abdusalyamova, M.; Makhmudov, F.; Eshov, B.; Kauzlarich, S., Thermal air-oxidized coating on $Yb_{14-x}RE_xMnSb_{11}$ ceramics. *Journal of Thermal Analysis and Calorimetry* **2018,** https://doi.org/10.1007/s10973-018-7659-z.
81. Brown, S. R.; Toberer, E. S.; Ikeda, T.; Cox, C. A.; Gascoin, F.; Kauzlarich, S. M.; Snyder, G. J., Improved thermoelectric performance in $Yb_{14}Mn_{1-x}Zn_xSb_{11}$ by the reduction of spin-disorder scattering. *Chemistry of Materials* **2008,** *20*, 3412-3419.
82. Toberer, E. S.; Cox, C. A.; Brown, S. R.; Ikeda, T.; May, A. F.; Kauzlarich, S. M.; Snyder, G. J., Traversing the Metal-Insulator Transition in a Zintl Phase: Rational Enhancement of Thermoelectric Efficiency in $Yb_{14}Mn_{1-x}Al_xSb_{11}$. *Advanced Functional Materials* **2008,** *18*, 2795-2800.
83. Cox, C. A.; Toberer, E. S.; Levchenko, A. A.; Brown, S. R.; Snyder, G. J.; Navrotsky, A.; Kauzlarich, S. M., Structure, Heat Capacity, and High-Temperature Thermal Properties of $Yb_{(14)}Mn_{(1-x)}Al_{(x)}Sb_{(11)}$. *Chemistry of Materials* **2009,** *21*, 1354-1360.
84. Star, K.; Zevalkink, A.; Huang, C.-K.; Dunn, B.; Fleurial, J.-P., Synthesis and Thermoelectric Properties of Doped $Yb_{14}MnSb_{11-x}Bi_x$ Zintls. *Mater. Res. Soc. Symp. Proc.* **2010,** *1267*, DD03-05.
85. Rauscher, J. F.; Cox, C. A.; Yi, T.; Beavers, C. M.; Klavins, P.; Toberer, E. S.; Snyder, G. J.; Kauzlarich, S. M., Synthesis, structure, magnetism, and high temperature thermoelectric properties of Ge doped $Yb_{14}MnSb_{11}$. *Dalton transactions* **2010,** *39*, 1055-62.
86. Yi, T.; Abdusalyamova, M. N.; Makhmudov, F.; Kauzlarich, S. M., Magnetic and transport properties of Te doped $Yb_{14}MnSb_{11}$. *Journal of Materials Chemistry* **2012,** *22*, 14378-14384.
87. Hu, Y.; Lee, K.; Kauzlarich, S., Optimization of $Ca_{14}MgSb_{11}$ through Chemical Substitutions on Sb Sites: Optimizing Seebeck Coefficient and Resistivity Simultaneously. *Crystals* **2018,** *8*, 211.
88. Xu, J.; Kleinke, H., Unusual Sb-Sb bonding in high temperature thermoelectric materials. *Journal of computational chemistry* **2008,** *29*, 2134-43.
89. Chan, J. Y.; Kauzlarich, S. M.; Klavins, P.; Shelton, R. N.; Webb, D. J., Colossal magnetoresistance in the transition-metal zintl compound $Eu_{14}MnSb_{11}$. *Chemistry of Materials* **1997,** *9*, 3132-3135.

90. Chan, J. Y.; Kauzlarich, S. M.; Klavins, P.; Shelton, R. N.; Webb, D. J., Colossal Negative Magnetoresistance in an Antiferromagnet. *Physical Review B* **1998,** *57*, 8103 - 8106.
91. Hu, Y. F.; Wang, J.; Kawamura, A.; Kovnir, K.; Kauzlarich, S. M., $Yb_{14}MgSb_{11}$ and $Ca_{14}MgSb_{11}$-New Mg-Containing Zintl Compounds and Their Structures, Bonding, and Thermoelectric Properties. *Chemistry of Materials* **2015,** *27*, 343-351.
92. Fisher, I. R.; Bud'ko, S. L.; Song, C.; Canfield, P. C.; Ozawa, T. C.; Kauzlarich, S. M., $Yb_{14}ZnSb_{11}$: charge balance in Zintl compounds as a route to intermediate Yb valence. *Physical Review Letters* **2000,** *85*, 1120-1123.
93. Akrap, A.; Barisic, N.; Forro, L.; Mandrus, D.; Sales, B. C., High-pressure resistivity and thermoelectric power in $Yb_{14}MnSb_{11}$. *Physical Review B* **2007,** *76*.
94. Srinath, S.; Poddar, P.; Srikanth, H.; Sales, B. C.; Mandrus, D., Observation of a new magnetic anomaly below the ferromagnetic curie temperature in $Yb_{14}MnSb_{11}$. *Physical Review Letters* **2005,** *95*.
95. Sales, B. C.; Jin, R. Y.; Mandrus, D.; Khalifah, P., Anomalous hall effect in three ferromagnetic compounds: $EuFe_4Sb_{12}$, $Yb_{14}MnSb_{11}$, and $Eu_8Ga_{16}Ge_{30}$. *Physical Review B* **2006,** *73*.
96. Burch, K. S.; Schafgans, A.; Butch, N. P.; Sayles, T. A.; Maple, M. B.; Sales, B. C.; Mandrus, D.; Basov, D. N., Optical study of interactions in a d-electron kondo lattice with ferromagnetism. *Physical Review Letters* **2005,** *95*.
97. Burch, K. S.; Chia, E. E. M.; Talbayev, D.; Sales, B. C.; Mandrus, D.; Taylor, A. J.; Averitt, R. D., Coupling between an optical phonon and the Kondo effect. *Physical Review Letters* **2008,** *100*.
98. Kuromoto, T. Y.; Kauzlarich, S. M.; Webb, D. J., A Novel Ferromagnet - $Ca_{14}MnBi_{11}$. *Molecular Crystals and Liquid Crystals* **1990,** *181*, 349-357.
99. Siemens, D. P.; Del Castillo, J.; Potter, W.; Webb, D. J.; Kuromoto, T. Y.; Kauzlarich, S. M., Specific heat of the ternary Zintl compounds ($Sr_{14}MnBi_{11}$ and $Ba_{14}MnBi_{11}$). *Solid State Communications* **1992,** *84*, 1029-31.
100. Rowe, D. M., Introduction. In *CRC Handbook of Thermoelectrics*, Rowe, D. M., Ed. CRC Press: New York, 1995.
101. Rowe, D. M., Ed., *CRC handbook of Thermoelectrics*. CRC Press: Boca Raton, FL, 1995; p 410.
102. Zhao, L. D.; Lo, S. H.; Zhang, Y.; Sun, H.; Tan, G.; Uher, C.; Wolverton, C.; Dravid, V. P.; Kanatzidis, M. G., Ultralow thermal conductivity and high thermoelectric figure of merit in SnSe crystals. *Nature* **2014,** *508*, 373-7.
103. Slack, G. A., New materials and performance limits for thermoelectrics In *CRC Handbook of Thermoelectrics*, Rowe, D. M., Ed. CRC Press: Boca Raton, FL, 1995; pp 407-440.
104. Toberer, E. S.; Zevalkink, A.; Snyder, G. J., Phonon engineering through crystal chemistry. *Journal of Materials Chemistry* **2011,** *21*, 15843-15852.
105. Kanatzidis, M. G., Advances in thermoelectrics: From single phases to hierarchical nanostructures and back. *MRS Bulletin* **2015,** *40*, 687-695.
106. Beretta, D.; Neophytou, N.; M.Hodges, J.; G.Kanatzidis, M.; Narducci, D.; Martin-Gonzalez, M.; Beekman, M.; Balke, B.; Cerretti, G.; Tremel, W.; Zevalkink, A.; I.Hofmann, A.; Müller, C.; Dörling, B.; Campoy-Quiles, M.; Caironia, M., Thermoelectrics: From history, a window to the future. *Materials Science and Engineering : R: Reports* **2018,** *in press*.
107. Snyder, G. J.; Christensen, M.; Nishibori, E.; Caillat, T.; Iversen, B. B., Disordered zinc in Zn_4Sb_3 with phonon-glass and electron-crystal thermoelectric properties. *Nature materials* **2004,** *3*, 458-63.
108. Girard, S. N.; He, J.; Zhou, X.; Shoemaker, D.; Jaworski, C. M.; Uher, C.; Dravid, V. P.; Heremans, J. P.; Kanatzidis, M. G., High performance Na-doped PbTe-PbS thermoelectric materials: electronic density of states modification and shape-controlled nanostructures. *Journal of the American Chemical Society* **2011,** *133*, 16588-97.

109. Hsu, K. F.; Loo, S.; Guo, F.; Chen, W.; Dyck, J. S.; Uher, C.; Hogan, T.; Polychroniadis, E. K.; Kanatzidis, M. G., Cubic AgPb(m)SbTe(2+m): bulk thermoelectric materials with high figure of merit. *Science* **2004,** *303*, 818-21.
110. Dolyniuk, J.-A.; Owens-Baird, B.; Wang, J.; Zaikina, J. V.; Kovnir, K., Clathrate thermoelectrics. *Materials Science and Engineering: R: Reports* **2016,** *108*, 1-46.
111. Grebenkemper, J. H.; Hu, Y.; Barrett, D.; Gogna, P.; Huang, C.-K.; Bux, S. K.; Kauzlarich, S. M., High Temperature Thermoelectric Properties of $Yb_{14}MnSb_{11}$ Prepared from Reaction of MnSb with the Elements. *Chemistry of Materials* **2015,** *27*, 5791-5798.
112. May, A. F.; Fleurial, J.-P.; Snyder, G. J., Thermoelectric performance of lanthanum telluride produced via mechanical alloying. *Physical Review B* **2008,** *78*.
113. Lee, E. K.; Yin, L.; Lee, Y.; Lee, J. W.; Lee, S. J.; Lee, J.; Cha, S. N.; Whang, D.; Hwang, G. S.; Hippalgaonkar, K.; Majumdar, A.; Yu, C.; Choi, B. L.; Kim, J. M.; Kim, K., Large thermoelectric figure-of-merits from SiGe nanowires by simultaneously measuring electrical and thermal transport properties. *Nano letters* **2012,** *12*, 2918-23.
114. Caillat, T.; Firdosy, S.; Li, B.; Ravi, V.; Paik, J.-A.; Nakatsukasa, G.; Chen-Kuo; Huang; Uhl, D.; Keyawa, N.; Chase, J.; Fleurial, J.-P., Progress Status Of The Development Of High-Efficiency Segmented Thermoelectric Couples. In *Joint Propulsion Conferences, 11th International Energy Conversion Engineering Conference*, AIAA 2013: San Jose, CA, 2013; p 3928 (+6).
115. Möchel, A.; Sergueev, I.; Wille, H. C.; Juranyi, F.; Schober, H.; Schweika, W.; Brown, S. R.; Kauzlarich, S. M.; Hermann, R. P., Lattice dynamics in the thermoelectric Zintl compound $Yb_{14}MnSb_{11}$. *Physical Review B* **2011,** *84*, 184303.
116. Bux, S. K.; Fleurial, J.-P.; Caillat, T.; Li, B. C. Y.; Star, K.; Firdosy, S.; Ravi, V.; Huang, C.-K.; Cheng, B.; Gogna, P.; Ma, J.; Allmen, P. v.; Vo, T. In *Engineering of Novel Thermoelectric Materials and Devices for Next Generation, Long Life, 20% Efficient Space Power Systems*, 11th International Energy Conversion Engineering Conference, Joint Propulsion Conferences, San Jose, CA, American Institute of Aeronautics and Astronautics: San Jose, CA, 2013; p 3927.
117. Yu, C.; Zhu, T. J.; Yang, S. H.; Shen, J. J.; Zhao, X. B., Preparation and thermoelectric properties of polycrystalline nonstoichiometric $Yb_{14}MnSb_{11}$ Zintl compounds. *physica status solidi (RRL) - Rapid Research Letters* **2010,** *4*, 212-214.
118. Ravi, V.; Firdosy, S.; Caillat, T.; Brandon, E.; Van Der Walde, K.; Maricic, L.; Sayir, A., Thermal Expansion Studies of Selected High-Temperature Thermoelectric Materials. *Journal of Electronic Materials* **2009,** *38*, 1433-1442.
119. Nesbitt, J. A., Rate of Sublimation of $Yb_{14}MnSb_{11}$, a Thermoelectric Material for Space Power Applications. *Journal of Electronic Materials* **2014,** *43*, 3128-3137.
120. Yu, C.; Chen, Y.; Xie, H.; Snyder, G. J.; Fu, C.; Xu, J.; Zhao, X.; Zhu, T., Improved Thermoelectric Properties in Lu-doped $Yb_{14}MnSb_{11}$ Zintl Compounds. *Applied Physics Express* **2012,** *5*, 031801.
121. May, A. F.; Snyder, G. J., Introduction to Modeling Thermoelectric Transport at High Temperatures. In *Materials, Preparation, and Characterization in Thermoelectrics*, Rowe, D. M., Ed. CRC Press: Boca Raton, 2012; pp 11-1-11-18.
122. Kuo, J. J.; Kang, S. D.; Imasato, K.; Tamaki, H.; Ohno, S.; Kanno, T.; Snyder, G. J., Grain boundary dominated charge transport in Mg3Sb2-based compounds. *Energy & Environmental Science* **2018,** *11*, 429-434.
123. Zevalkink, A.; Zeier, W. G.; Cheng, E.; Snyder, J.; Fleurial, J.-P.; Bux, S., Nonstoichiometry in the Zintl Phase $Yb_{1-\delta}Zn_2Sb_2$ as a Route to Thermoelectric Optimization. *Chemistry of Materials* **2014,** *26*, 5710-5717.
124. Star, K. Synthesis and Characterization of 14-1-11 Ytterbium Manganese Antimonide Derivatives for Thermoelectric Applications. UCLA, 2013.

125. Kazem, N.; Zaikina, J. V.; Ohno, S.; Snyder, G. J.; Kauzlarich, S. M., Coinage-Metal-Stuffed $Eu_9Cd_4Sb_9$: Metallic Compounds with Anomalous Low Thermal Conductivities. *Chemistry of Materials* **2015,** *27*, 7508-7519.
126. Jonker, G. H., The application of combined conductivity and Seebeck-effect plots for the analysis of semiconductor properties. *Philips Res. Repts* **1968,** *23*, 131-138.

TOC

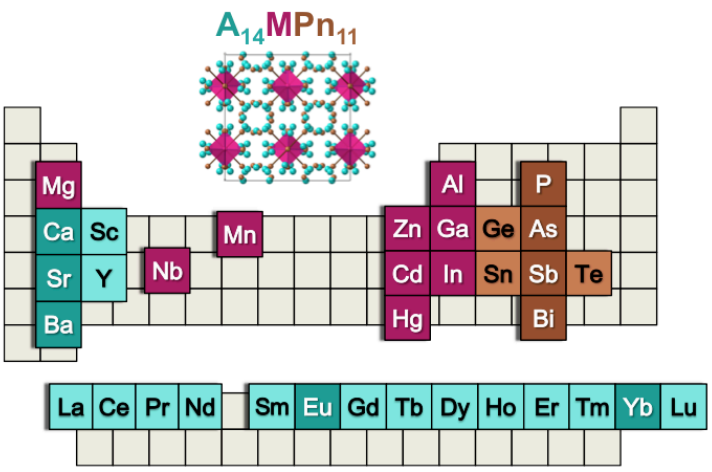

Add/subtract electrons → tune magnetic, electronic, and transport properties